LI
LABORATORY INVESTIGATION
THE BASIC AND TRANSLATIONAL PATHOLOGY RESEARCH JOURNAL
VOLUME 100 | SUPPLEMENT 1 | MARCH 2020

ABSTRACTS

PATHOBIOLOGY AND EMERGING TECHNIQUES (1802-1841)

FEBRUARY 29-MARCH 5, 2020

LOS ANGELES CONVENTION CENTER
LOS ANGELES, CALIFORNIA

Published by
SPRINGER NATURE
www.ModernPathology.org

USCAP Creating a Better Pathologist
AN OFFICIAL JOURNAL OF THE UNITED STATES AND CANADIAN ACADEMY OF PATHOLOGY

EDUCATION COMMITTEE

Jason L. Hornick, Chair

Rhonda K. Yantiss, Chair, Abstract Review Board and Assignment Committee

Laura W. Lamps, Chair, CME Subcommittee

Steven D. Billings, Interactive Microscopy Subcommittee

Raja R. Seethala, Short Course Coordinator

Ilan Weinreb, Subcommittee for Unique Live Course Offerings

David B. Kaminsky (Ex-Officio)

Zubair Baloch
Daniel Brat
Ashley M. Cimino-Mathews
James R. Cook
Sarah Dry
William C. Faquin
Yuri Fedoriw
Karen Fritchie
Lakshmi Priya Kunju
Anna Marie Mulligan
Rish K. Pai
David Papke, Pathologist-in-Training
Vinita Parkash
Carlos Parra-Herran
Anil V. Parwani
Rajiv M. Patel
Deepa T. Patil
Lynette M. Sholl
Nicholas A. Zoumberos, Pathologist-in-Training

ABSTRACT REVIEW BOARD

Benjamin Adam
Narasimhan Agaram
Rouba Ali-Fehmi
Ghassan Allo
Isabel Alvarado-Cabrero
Catalina Amador
Roberto Barrios
Rohit Bhargava
Jennifer Boland
Alain Borczuk
Elena Brachtel
Marilyn Bui
Eric Burks
Shelley Caltharp
Barbara Centeno
Joanna Chan
Jennifer Chapman
Hui Chen
Beth Clark
James Conner
Alejandro Contreras
Claudiu Cotta
Jennifer Cotter
Sonika Dahiya
Farbod Darvishian
Jessica Davis
Heather Dawson
Elizabeth Demicco
Katie Dennis
Anand Dighe
Suzanne Dintzis
Michelle Downes
Andrew Evans
Michael Feely
Dennis Firchau
Gregory Fishbein
Andrew Folpe
Larissa Furtado
Billie Fyfe-Kirschner
Giovanna Giannico
Anthony Gill
Paula Ginter
Tamara Giorgadze
Purva Gopal
Anuradha Gopalan
Abha Goyal
Rondell Graham
Alejandro Gru
Nilesh Gupta
Mamta Gupta
Gillian Hale
Suntrea Hammer
Malini Harigopal
Douglas Hartman
John Higgins
Mai Hoang
Mojgan Hosseini
Aaron Huber
Peter Illei
Doina Ivan
Wei Jiang
Vickie Jo
Kirk Jones
Neerja Kambham
Chiah Sui Kao
Dipti Karamchandani
Darcy Kerr
Ashraf Khan
Francesca Khani
Rebecca King
Veronica Klepeis
Gregor Krings
Asangi Kumarapeli
Alvaro Laga
Steven Lagana
Keith Lai
Michael Lee
Cheng-Han Lee
Madelyn Lew
Zaibo Li
Faqian Li
Ying Li
Haiyan Liu
Xiuli Liu
Yen-Chun Liu
Lesley Lomo
Tamara Lotan
Anthony Magliocco
Kruti Maniar
Emily Mason
David McClintock
Bruce McManus
David Meredith
Anne Mills
Neda Moatamed
Sara Monaco
Atis Muehlenbachs
Bita Naini
Dianna Ng
Tony Ng
Michiya Nishino
Scott Owens
Jacqueline Parai
Yan Peng
Manju Prasad
Peter Pytel
Stephen Raab
Joseph Rabban
Stanley Radio
Emad Rakha
Preetha Ramalingam
Priya Rao
Robyn Reed
Michelle Reid
Natasha Rekhtman
Jordan Reynolds
Michael Rivera
Andres Roma
Avi Rosenberg
Esther Rossi
Peter Sadow
Steven Salvatore
Souzan Sanati
Anjali Saqi
Jeanne Shen
Jiaqi Shi
Gabriel Sica
Alexa Siddon
Deepika Sirohi
Kalliopi Siziopikou
Sara Szabo
Julie Teruya-Feldstein
Khin Thway
Rashmi Tondon
Jose Torrealba
Andrew Turk
Evi Vakiani
Christopher VandenBussche
Paul VanderLaan
Olga Weinberg
Sara Wobker
Shaofeng Yan
Anjana Yeldandi
Akihiko Yoshida
Gloria Young
Minghao Zhong
Yaolin Zhou
Hongfa Zhu
Debra Zynger

To cite abstracts in this publication, please use the following format: **Author A, Author B, Author C, et al. Abstract title (abs#). In "File Title."** ***Laboratory Investigation*** **2020; 100 (suppl 1): page#**

1802 Clinical Validation of NGS Pan-Cancer ctDNA Assay for Detection of Microsatellite Instability

Wael Al Zoughbi[1], Eniko Papp[2], Shaham Beg[3], Erika Hissong[4], Evan Fernandez[3], Kenneth Eng[5], David Wilkes[3], Andrea Sboner[3], Olivier Elemento[6], Juan Miguel Mosquera[3]

[1]Weill Cornell Medicine, New York City, NY, [2]Personal Genome Diagnostics (PGDx), Baltimore, MD, [3]Weill Cornell Medicine, New York, NY, [4]New York-Presbyterian/Weill Cornell Medical Center, New York, NY, [5]Englander Institute for Precision Medicine, Brooklyn, NY, [6]New York, NY

Disclosures: Wael Al Zoughbi: None; Eniko Papp: None; Shaham Beg: None; Erika Hissong: None; Evan Fernandez: None; Kenneth Eng: None; David Wilkes: None; Andrea Sboner: None; Olivier Elemento: None; Juan Miguel Mosquera: *Grant or Research Support*, Personal Genome Diagnostics (PGDx)

Background: Defective DNA mismatch repair (dMMR) system that results in microsatellite instability (MSI), is a predictive biomarker for tumor- immunotherapy response to programmed cell death protein 1 (PD-1) inhibitors. A Next Generation Sequencing (NGS)-based approach to assess MSI in circulating tumor DNA (ctDNA) is underutilized. We provide clinical evidence for MSI detection in plasma and highlight its utility to inform clinical decisions in metastatic disease.

Design: From our pan-cancer NGS-based precision medicine cohort, we selected 113 patients with known MSI phenotype assessed on tissue specimens by IHC, PCR, and whole-exome sequencing (WES). MSISensor score from WES data was interpreted as: < 2.5: microsatellite stable (MSS); >2.5 and <6: Indeterminate (requires orthogonal validation); > 6: microsatellite instability-high (MSI-H). DNA was extracted from plasma samples and sequenced using a molecular barcoded NGS assay (*PGDx elio plasma resolve*). The assay requires (≥ 40ng) DNA and applies multifactor error suppression methods combined with a distribution modeling and a peak-finding algorithm to reduce background error rates and identify the specific mononucleotide sequences in 9 monoallelic regions. ctDNA MSI status was defined as either MSI-H or indeterminate.

Results: From the 113 selected patients, 13 tumor samples had tissue MSISensor score > 2.5 (Table). MSI status on plasma was compared. We found concordance between ctDNA and MSI calls from matched tissue samples in (9/13) cases (69.2%): (3) has MSI-H phenotype; (6) defined as indeterminate. Among the four discrepant results (3) were called MSI-H by MSISensor, but indeterminate based on the ctDNA assay. The fourth case was called MSI-H based on *PGDx elio plasma resolve* assay, but indeterminate based on the MSISensor score (MSISensor score = 4.93). Importantly, IHC and PCR results for this case confirmed the MSI-H phenotype. This patient was diagnosed with metastatic prostate cancer and received Pembrolizumab after failed responses to both androgen-deprivation therapy and chemotherapy. Clinical and radiological response has been comp

ID	MSISensor (Tissue)	Tissue MSI Status[#]	PGDx elio Plamsa MSI Status	Tumor Type	Primary/Metastatic
1	**2.96**	Indeterminate	Indeterminate	Adrenal Cortical Carcinoma	Metastatic
2	**3.67**	Indeterminate	Indeterminate	Colorectal Adenocarcinoma	Metastatic
3	**3.71**	Indeterminate	Indeterminate	Urothelial Carcinoma	Metastatic
4	**4.05**	Indeterminate	Indeterminate	Prostatic Adenocarcinoma	Primary
5	**4.29**	Indeterminate	Indeterminate	Renal Cell Carcinoma	Metastatic
6	**4.93**	Indeterminate	MSI-H	Prostatic Adenocarcinoma	Metastatic
7	**5.01**	Indeterminate	Indeterminate	Thymic Carcinoma	Metastatic
8	**9.14**	MSI-H	Indeterminate	Colorectal Medullary Carcinoma	Primary
9	**9.31**	MSI-H	MSI-H	Gastric Adenocarcinoma	Primary
10	**10.73**	MSI-H	MSI-H	Colorectal Adenocarcinoma	Metastatic
11	**18.18**	MSI-H	Indeterminate	Colorectal Adenocarcinoma	Metastatic
12	**20**	MSI-H	Indeterminate	Colorectal Adenocarcinoma	Primary
13	**20.59**	MSI-H	MSI-H	Colorectal Adenocarcinoma	Primary

Table: MSI status calls from NGS sequencing of DNA extracted from tumor tissue sample (WES)

or NGS sequencing of ctDNA.

[#] MSISensor score > 2.5 and <6: Indeterminate; > 6: Microsatellite Instability-High (MSI-H)

Figure 1 - 1802

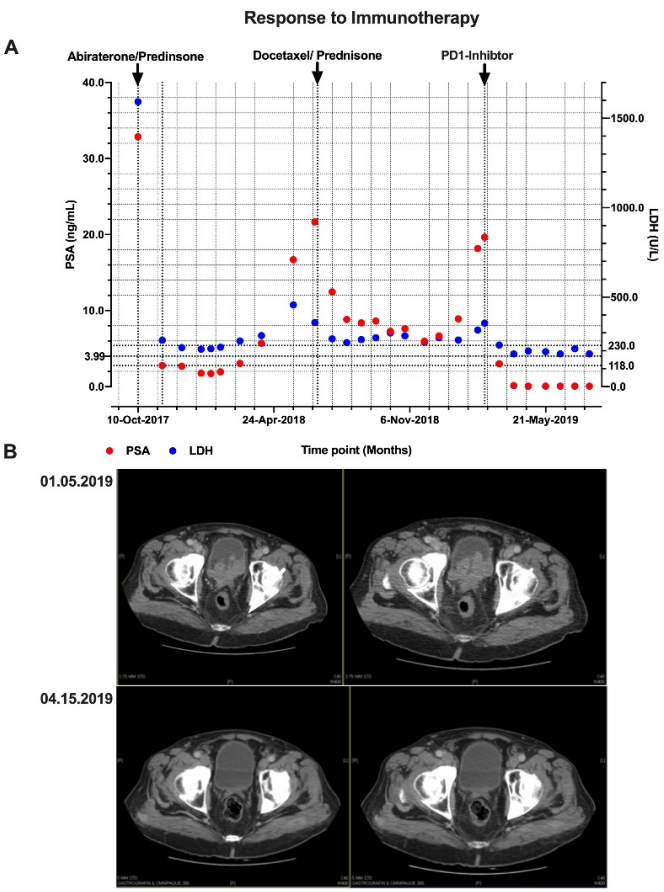

Figure. **Clinical and radiological response assessment of immunotherapy**. **A)** Prostate-specific antigen (PSA) and Lactate dehydrogenase (LDH) levels decreased after Pembrolizumab (PD-1 inhibitor) treatment and remined within the normal levels (upper panel). **B)** Images in lower panel demonstrate a prominent radiological response to Pembrolizumab compared to images before starting immunotherapy (upper panel).

Conclusions: Assessment of microsatellite status on ctDNA is practical. Estimating the specificity and sensitivity of this test requires larger validation studies, currently ongoing. Such plasma-based assay has potential application in the clinic to guide immunotherapy decision in advanced cancer patients, particularly when tissue specimens are not available or insufficient to evaluate dMMR or MSI-H phenotype.

1803 Visualization of the Effect of Assay Size on the Uncertainty of Tumor Mutational Burden Measurement Using Targeted Sequencing Panels

Nathanael Bailey, University of Pittsburgh Medical Center, Pittsburgh, PA

Disclosures: Nathanael Bailey: None

Background: Tumor mutational burden (TMB) is defined by the number of somatic mutations present in a tumor. TMB is an emerging therapeutic biomarker that is a continuous variable associated with response to immune checkpoint inhibitors (ICI); tumors with higher TMB exhibit better responses to ICIs. While criteria are not well established, thresholds ranging from 10 mutations/megabase (mut/Mb) to 20 mut/Mb are commonly reported in the literature to dichotomize tumors into TMB-low and TMB-high categories.

Although TMB is defined as the exomic mutation count, few tumors currently have exome sequencing performed. Rather, mutations are enumerated in targeted sequencing assays, and this number is divided by the assay exomic coverage to determine TMB. The uncertainty of this TMB result is dependent upon the exomic coverage of the specific assay, and TMB values generated by current assays that sequence ~1 Mb of exome retain a significant degree of uncertainty near the clinically relevant range of 10-20 mut/Mb due to sampling error. This uncertainty may be difficult to conceptualize, so we set out to make an application that displays TMB measurement uncertainty given user-defined inputs.

Design: A web app was written that takes a TMB value and assay size as user inputs. The app additionally draws on publicly available mutational data for patients treated with ICI from cBioportal (Samstein et al. Nat Genet 2019, Cerami et al. Cancer Discov 2012, Gao et al. Sci Signal 2013) to generate prior distributions for TMB in different tumor types and histology-specific TMB deciles. The app displays the uncertainty (90% confidence interval) of the TMB result using the binomial distribution and the user-inputted data. At the user's discretion, the app can also incorporate prior information regarding histology-specific TMB distributions to visualize the impact of this knowledge on the TMB result using a Bayesian approach.

Results: Example app outputs are displayed in the figures, demonstrating the significant uncertainty of a result of 8 mut/Mb, and the impact of increasing assay coverage on the confidence interval. The app is available for use at: https://pathology.shinyapps.io/tmbapp/.

Figure 1 - 1803

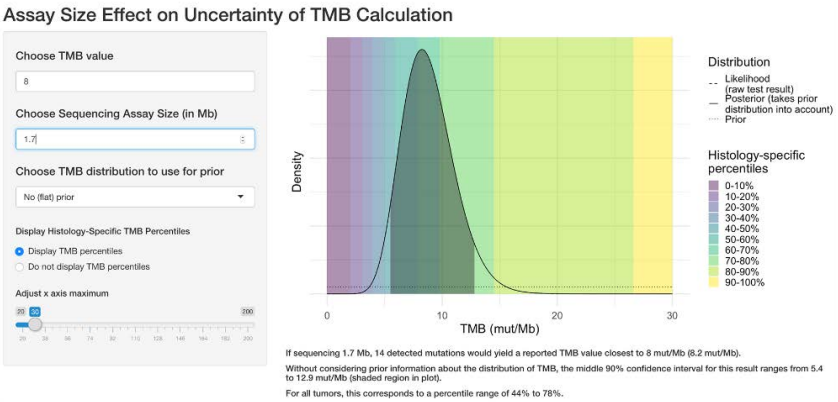

Figure 2 - 1803

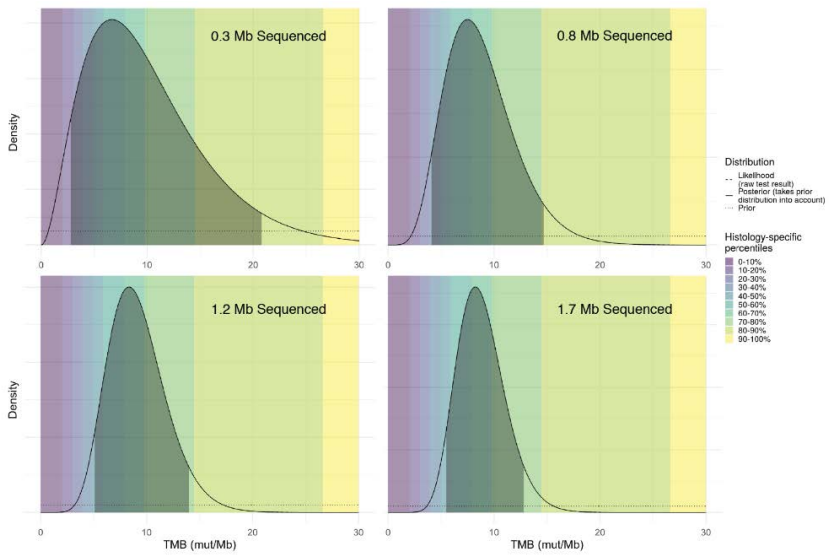

Effect of panel size when ~ 8 mut/Mb detected. The shaded areas display the 90% middle confidence interval for the result, demonstrating broad uncertainty even when large targeted panels are used.

Conclusions: The app provides a convenient way to visualize the uncertainty of a TMB result due to sampling error. Other sources of error are not reflected in the output. Laboratories reporting TMB should consider acknowledging the uncertainty of TMB results in their reports, particularly near potentially clinically relevant thresholds.

1804 Continuity of Interstitial Spaces within Skin and Colon and with Their Underlying Fascia: Pathways for Spread of Malignancy and Infection

Odise Cenaj[1], Douglas Allison[2], Briana Zeck[2], Lilly Drohan[3], Luis Chiriboga[4], Young Nyun Park[5], Neil Theise[2]
[1]New York University Langone Health, New York, NY, [2]NYU Langone Health, New York, NY, [3]Colgate University, Hamilton, NY, [4]New York University, New York, NY, [5]Yonsei University College of Medicine, Seoul, Korea, Republic of South Korea

Disclosures: Odise Cenaj: None; Douglas Allison: None; Briana Zeck: None; Lilly Drohan: None; Luis Chiriboga: None; Young Nyun Park: None; Neil Theise: None

Background: Fibroconnective tissues of the body are traditionally conceived as layers of densely compacted collagen. Recent *in vivo* microscopy, however, demonstrates that at least some, including visceral submucosae, dermis, fascia, adventitia and perineurium, are actually a reticular network of fluid-filled sinuses supported by a complex scaffold of thick collagen bundles (Benias et al *Sci Rep* 2018: 8). The interstitial fluid is rich in hyaluronic acid (HA). Whether these large scale interstitial spaces are continuous between tissues/organs or separate is unclear. Continuity was investigated by two methods: 1. movement of non-biological pigment (tattoo pigment, colloidal silver) in colon and skin specimens; 2. localization of HA by IHC.

Design: H&E-stained sections of FFPE tissues from resected colons following endoscopic submucosal tattoo for malignant polyps (n=5) and from skin biopsies with either cosmetic tattoos (n=3) or colloidal silver (n=2) were examined. Location of particles was assessed. The slides were then scanned, decolorized, and stained by multiplex chromogenic IHC assay (Discovery Ultra, Ventana) for HA-binding protein (brown), vimentin (magenta) and CD34 (teal) to label interstitial lining cells.

Results: Tattoo pigment and colloidal silver within the interstitial spaces was identified in the dermis (Fig. 1) and colonic submucosa and in the dependent mesenteric and subcutaneous fascias. In all colon specimens HA IHC highlighted the spatial continuity of all layers of the colon from lamina propria through muscularis mucosae to submucosa (Fig. 2A), then through the muscularis propria into mesenteric fascia (Fig. 2B, C). Continuity between these spaces and perivascular stroma/adventitia and perineurium in the bowel wall was also evident. Continuity of HA-filled spaces is also demonstrated from papillary to reticular dermis and then to subcutaneous fascia interface.

Figure 1 - 1804

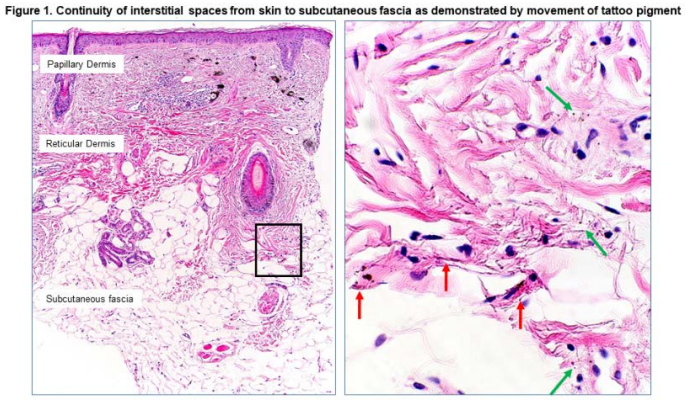

Figure 1 Legend. Continuity of interstitial spaces through dermis and into subcutaneous fascia.
Left panel: H&E section (10X) of skin and subcutaneous fascia with injected tattoo pigment. Note the presence of pigment particles within papillary and reticular dermis. **Right panel**: Higher magnification (40X) of rectangular focus demonstrating intracellular (**red arrows**) and extracellular (**green arrows**) tattoo pigment particles within interstitial spaces between collagen bundles of the reticular dermis and into subcutaneous fascia.

Figure 2 - 1804

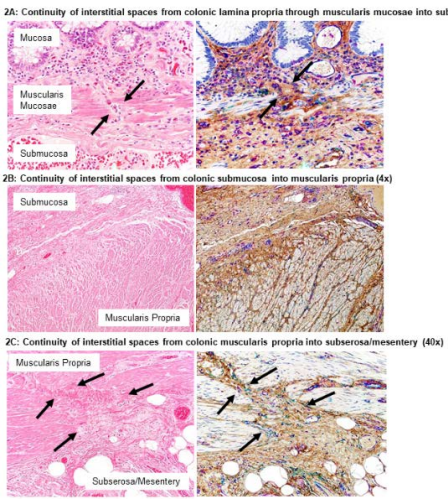

Figure 2 Legend. Continuity between interstitial spaces across all layers of the colon into the mesenteric soft tissues based on localization of hyaluronic acid.
Left panels: H&E sections of colon.
Right panels: Multiplex chromogenic immunohistochemistry of the same areas for hyaluronic acid (HA)-binding protein (brown), vimentin (magenta), and CD34 (teal). HA highlights interstitial space fluid. Vimentin stains mononuclear cells, CD34 stains endothelial cells lining capillaries, veins and arteries, while lining cells of the interstitial spaces stain for both CD34 and vimentin (overlap color is navy blue).

Conclusions: Interstitial spaces are neither virtual nor a result of processing artifact, but are filled with physiologically relevant fluid rich in HA. Their continuity across tissue compartments is demonstrated by movement of non-biological pigments and by spatial continuity of HA. The implications of such multisystem continuity are protean, but may particularly explain commonly observed modes of discontinuous cancer spread through tissue planes, such as mesenteric tumor deposits in colon cancer and subcutaneous in-transit melanoma metastasis, and spread of infection (e.g. necrotizing fasciitis).

1805 SMA Diagnostic and Carrier Screening Testing by Droplet Digital PCR Reveals Occurrence of 5 Copy Numbers of SMN1, Substantiating Potential 3+0 Silent Carrier Status

Sara Cook[1], Noemi Vidal Folch[1], Linda Hasadsri[1], Devin Oglesbee[1]
[1]Mayo Clinic, Rochester, MN

Disclosures: Sara Cook: None; Noemi Vidal Folch: None; Linda Hasadsri: None; Devin Oglesbee: None

Background: Spinal muscular atrophy (SMA) is a neurodegenerative disease caused by a deletion in the survival motor neuron 1 (SMN1) gene. The survival motor neuron 2 (SMN2) gene varies from SMN1 such that only 10% of the protein is generated. Accordingly, SMN2 copy number correlates with disease severity. Our carrier screening method uses droplet digital PCR (ddPCR) to quantify copy numbers of SMN1 and SMN2. Other methods have high copy number limitations and do not report copy numbers higher than 4, whereas our method has the ability to quantify as high as 5 copy numbers. Detecting silent carriers (2+0) is a limitation of most methods. A ddPCR assay which counts copies of a single-nucleotide polymorphism in SMN1, g.27134T>G, NG_008691.1, reported to be a haplotype-specific marker for (2+0) carriers, was recently added to our method to ascertain an individual's risk for being a silent carrier. We sought to determine the prevalence of individuals with 5 or more copies of SMN1and to determine whether these individuals are positive for the polymorphism.

Design: We retrospectively reviewed test results from the carrier screening and diagnostic ddPCR assay ran from March 2018 to August 2019. In total, we collected SMN1 and SMN2 copy number data for 4,438 individuals. We then performed g.27134T>G ddPCR analysis on samples that tested positive for 5 or more copy numbers of SMN1.

Results: We determined that 2 individuals within this cohort tested positive for 5 copy numbers of SMN1 indicating that 5 copy numbers of SMN1 occurs with a prevalence of 0.05%. Notably, these individuals had 0 copy number of SMN2. g.27134T>G ddPCR analysis of these 2 individuals resulted as 3/5 and 1/5 copy numbers positive for the g.27134T>G polymorphism.

	SMN 2 copy number						
SMN1 copy number		**0**	**1**	**2**	**3**	**4**	**5**
	0	0	2	18	14	9	0
	1	4	35	66	19	8	0
	2	280	1443	1971	80	7	1
	3	83	259	83	9	0	0
	4	35	6	4	0	0	0
	5	2	0	0	0	0	0

Conclusions: Our findings have important implications in carrier screening. Our data suggests that the status of the individuals with 5 copy numbers in our study likely include a (3+2) status as they both tested positive for the polymorphism. This reveals the possibility of silent SMN1 (3+0) carriers amongst individuals testing positive for 3 copy numbers of SMN1 in carrier screening. Furthermore, atypical copy numbers of SMN1 can affect the risk and clinical severity of other neurological disorders including amyotrophic lateral sclerosis and progressive muscular atrophy. This highlights the importance of determining the prevalence of high SMN1 copy number status in the general population.

1806 Ovarian Cancer Tumor Derived Explants - A Platform to Test Therapeutical Targets

Delfim Doutel[1], Fernanda Silva[2], Rita Mendes[3], Maria Mendes[4], Sofia Abreu[3], Ines Isidro[3], Erwin Boghaert[5], Catarina Brito[3], Ana Félix[6]

[1]Instituto Português de Oncologia de Lisboa Francisco Gentil (IPOLFG), Lisboa, Portugal, [2]NOVA Medical School, Queijas, Portugal, [3]iBET, Instituto de Biologia Experimental e Tecnológica & Instituto de Tecnologia Química e Biológica António Xavier, Oeiras, Portugal, [4]iBET, Instituto de Biologia Experimental e Tecnológica & Instituto de Tecnologia Química e Biológica António Xavier, Lisboa, Portugal, [5]ABBVIE, North Chicago, IL, [6]Instituto Português de Oncologia de Lisboa/CEDOC, Lisboa, Portugal

Disclosures: Delfim Doutel: None; Fernanda Silva: None; Rita Mendes: None; Maria Mendes: None; Sofia Abreu: None; Ines Isidro: None; Erwin Boghaert: *Employee*, AbbVie; *Employee*, AbbVie; Catarina Brito: *Grant or Research Support*, AbbVie, Merck KGaA; Ana Félix: None

Background: Epigenetic and immunological dysregulations are commonly associated with cancer. The use of histone deacetylases (HDACs) and PD-L1 inhibitors represent promising novel therapeutic approaches.

We developed a platform of ovarian carcinoma patient-derived explants (PDE) to evaluate drug efficacy and improve therapy assignment. Here our goal was to verify the ability to preserve biomarkers in long-term cultures.

Design: Two mirrored samples from 13 ovarian high-grade serous carcinoma (HGSC), 3 cases with neoadjuvant chemotherapy, were collected. One was saved for control and the other mechanically dissociated into fragments (125mm3) and cultured under orbital agitation. Immunohistochemical study of primary HGSC and PDE with 21-30 days of culture growth evaluated HDAC 1, 2, 3, 4, 6, 7 and 8, pHDAC 3, pHDAC4/5/7 and PD-L1 (E1L3N) expression. For the primary HGSC, we also tested two PD-L1 clones: 2C33 (extracellular domain) and E1L3N (cytoplasmatic domain). PD-L1 expression on tumor cells was scored as absent (<1%), weak (1-5%), moderate (6-50%) and strong (>50%). The remaining markers were scored as <1%, 1-5%, 6-25%, 26-50%, 51-75% and >75%.

Results: PDE retained the original tumor architecture and main cellular components, namely epithelial cells and fibroblasts for at least one month of culture. Immunohistochemistry results are presented in Figure 1 and 2. The concordance was high for HDAC1 (100%); pHDAC4/5/7 (92%); pHDAC3 (85%); moderate for HDAC2 and HDAC4 (69%); HDAC6 and HDAC8 (61%); HDAC3 (53%); and low for HDAC7 (23%). HDAC2, 3, 8 and pHDAC3; and HDAC4, 6, 7 pHDAC4/5/7 were commonly more and less expressed on PDE, respectively. HDAC expression was discordant between same patient HGSC and PDE in up to 6 HDACs. The expression of both PD-L1 clones in the HGSC was similar, with 1 non-concordant case, in which the disparity was weak versus absent. The concordance between HGSC and PDE samples for PD-L1(E1L3N) was moderate (8/13 cases), the largest disparity being moderate versus absent.

Figure 1 - 1806

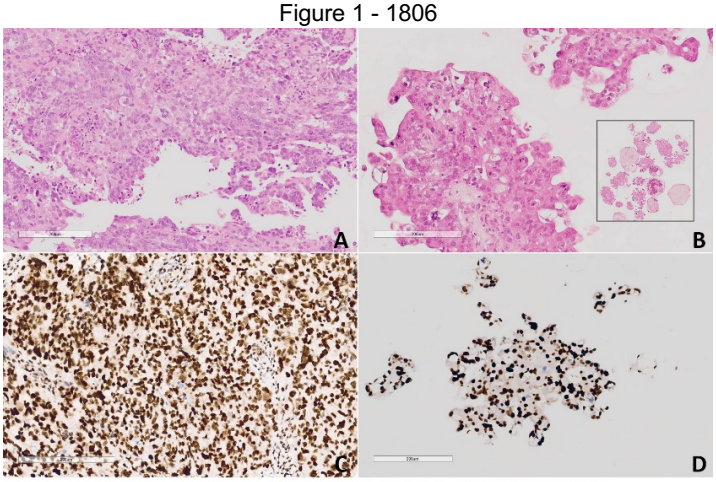

Fig.1: A - HGSC H&E; B - PDE H&E; C - HGSC HDAC1 expression; D - PDE HDAC1 expression.

Figure 2 - 1806

Case Nº	2C33	E1L3N	HDAC1		HDAC2		HDAC3		pHDAC3		HDAC4		HDAC6		HDAC7		pHDAc457		HDAC8	
	HGSC	HGSC	HGSC	PDE	HGSC	PDE	HGSC	PDE	HGSC	PDE	HGSC	PDE	HGSC	PDE	HGSC	PDE	HGSC	PDE	HGSC	PDE
1	6-50%	6-50%	>75%	>75%	>75%	>75%	6-25%	>75%	1-5%	>75%	51-75%	>75%	51-75%	51-75%	<1%	<1%	>75%	>75%	<1%	>75%
2	1-5%	<1%	>75%	>75%	>75%	>75%	>75%	>75%	>75%	>75%	>75%	>75%	6-25%	<1%	26-50%	1-5%	>75%	>75%	>75%	>75%
3	<1%	<1%	>75%	>75%	>75%	>75%	>75%	>75%	>75%	>75%	>75%	>75%	>75%	1-5%	26-50%	<1%	>75%	>75%	>75%	>75%
4	<1%	<1%	>75%	>75%	>75%	>75%	>75%	>75%	>75%	>75%	>75%	>75%	>75%	51-75%	>75%	>75%	>75%	>75%	>75%	>75%
5	<1%	<1%	>75%	>75%	<1%	>75%	6-25%	>75%	>75%	>75%	>75%	>75%	>75%	>75%	<1%	<1%	51-75%	>75%	>75%	>75%
6	<1%	<1%	>75%	>75%	51-75%	>75%	51-75%	>75%	>75%	>75%	>75%	>75%	>75%	>75%	26-50%	>75%	>75%	>75%	26-50%	>75%
7	<1%	<1%	>75%	>75%	>75%	>75%	>75%	>75%	51-75%	51-75%	>75%	>75%	>75%	>75%	51-75%	26-50%	>75%	>75%	>75%	>75%
8	<1%	<1%	>75%	>75%	>75%	>75%	>75%	>75%	51-75%	>75%	6-25%	51-75%	>75%	>75%	6-25%	26-50%	>75%	>75%	6-25%	6-25%
9	<1%	<1%	>75%	>75%	>75%	>75%	>75%	6-25%	>75%	>75%	>75%	1-5%	>75%	51-75%	51-75%	26-50%	>75%	>75%	51-75%	>75%
10	<1%	<1%	>75%	>75%	6-25%	>75%	51-75%	>75%	>75%	>75%	>75%	51-75%	6-25%	6-25%	26-50%	1-5%	>75%	1-5%	>75%	>75%
11	<1%	<1%	>75%	>75%	>75%	>75%	>75%	26-50%	>75%	>75%	>75%	>75%	>75%	>75%	(-)	<1%	>75%	>75%	26-50%	>75%
12	1-5%	1-5%	>75%	>75%	>75%	>75%	>75%	>75%	>75%	>75%	>75%	>75%	>75%	>75%	>75%	26-50%	>75%	>75%	26-50%	>75%
13	6-50%	6-50%	>75%	>75%	<1%	>75%	>75%	>75%	>75%	>75%	>75%	>75%	>75%	6-25%	>75%	<1%	51-75%	51-75%	>75%	>75%

Fig. 2 – Table with PD-L1 and HDACs results. (-): Not evaluated.

Conclusions: PD-L1 expression in ovarian high grade serous carcinoma is low and has little variability between original tumor and the explants. Both PD-L1 clones in HGSC show similar results. Also, HDAC expression is generally preserved in PDE, notably on HDAC1 and pHDACs. Our study supports PDEs as a useful tool in oncologic research due to general preservation of original tumor biomarkers and characteristics.

This work was funded by iNOVA4Health, FCT/MEC and AbbVie.

1807 DUET: Dual-Mode Emission and Transmission Microscopy for Collagen Detection on H&E Slides

Farzad Fereidouni[1], Austin Todd[1], Casey Gilles[2], Che-Wei Chang[1], James Chan[1], Alexander Borowsky[3], Souvik Sarkar, Kuang-Yu Jen[1], Karen Matsukuma[1], Richard Levenson[4]
[1]University of California Davis, Sacramento, CA, [2]University of California Los Angeles, Carmichael, CA, [3]Davis, CA, [4]UC Davis Health, Sacramento, CA

Disclosures: Farzad Fereidouni: *Stock Ownership*, HistoliX; Austin Todd: None; Casey Gilles: None; Che-Wei Chang: None; James Chan: None; Alexander Borowsky: None; Souvik Sarkar: None; Kuang-Yu Jen: None; Karen Matsukuma: None; Richard Levenson: *Stock Ownership*, HistoliX, Inc.

Background: In the clinical practice of pathology, special stains are commonly used to highlight collagen and to help evaluate fibrosis. Such stains can show inconsistencies from lab to lab and day to day, increasing the variability of interpretation. Moreover, generating

special stained slides requires additional tissue sections, special reagents, and staining steps, which could add to cost, time, and workflow complications. We have developed a new microscopy approach, termed DUET (DUal-mode Emission and Transmission) that can be used to extract collagen signals directly from existing H&E slides.

Design: Our innovation involves utilization of additional signals present in fluorescence images of H&E slides. These can be combined with a simultaneously acquired brightfield image to create a virtual special-stain result. The prototype hardware consists of a custom scanner that employs a simple wide-field imaging setup combining brightfield and fluorescence illumination modules. Two images are acquired. First, in brightfield mode, the slide is illuminated from the bottom with a white light LED and a regular transmission histology image is acquired. Next, the same region is illuminated with LED-derived excitation light and a fluorescence image is acquired with a 9-megapixel color camera. By spectrally unmixing the collagen signal from the other components in the image, it is possible to display it in its own channel. Moreover, the collagen signal can be overlaid on the traditional H&E image to create virtual special-stained slide.

Results: Pixel-registered brightfield and fluorescence images of H&E-stained slides from kidney, liver and breast cancer were acquired using DUET. We demonstrate the possibility of extracting the collagen distribution reliably from H&E slides and we compare the specificity to existing methods including trichrome, picrosirius red, immunohistochemistry and second-harmonics generation microscopy.

Figure 1 - 1807

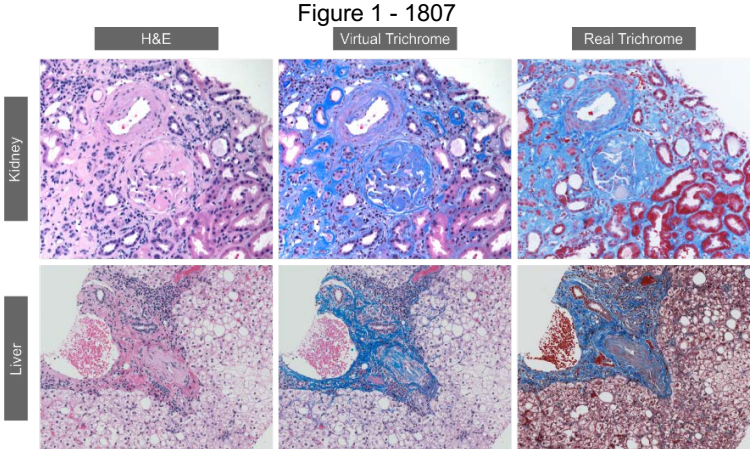

Conclusions: We demonstrate that a simple, novel approach using dual-mode imaging of standard H&E-stained sections, combining brightfield and fluorescence, can reveal high-quality, spatially resolved collagen (and basement-membrane) signals without requiring special stains, expensive optics, or preparation of extra slides. DUET is suitable for translation into clinical settings owing to its low cost and complexity, and rapid imaging performance. It can also be extended to provide additional value when used to image frozen sections that are currently n

1808 A Machine Learning-Based Method for the Prediction of Blast Count on Bone Marrow Aspirate in Myelodysplastic Syndromes and Acute Myeloid Leukemia

May Fu[1], Xinyan Fu[2], Hong Yuan[3], Guoping Zhang[4], Shihong Zhang[5], Xiangui Peng[6], Zhen Wang[7], Hongyang Zhang[8], Fengqi Fang[9], Xinyi Cao[2], Mingyi Chen[10]

[1]University of Texas Southwestern, Dallas, TX, [2]Hangzhou Zhi-wei Information&Technology Ltd., Hangzhou, Zhejiang, China, [3]First Affiliated Hospital of Dalian Medical University, Dalin, Liaoning, China, [4]Department of Hematology, Xiangya Hospital of Central South University, Changsha, Hunan, China, [5]The First Affiliated Hospital of Sun Yat-sen University, Guangzhou, Guangdong, China, [6]Xinqiao Hospital, Chongqing, Chongqing, China, [7]First Affiliated Hospital of Dalian Medical University, Dalian, Liaoning, China, [8]Hematology Department, The Xinqiao Hospital of Army Medical University, Chongqing, Chongqing, China, [9]The First Affiliated Hospital Of Dalian Medical University, Dalian, Liaoning, China, [10]University of Texas Southwestern Medical Center, Dallas, TX

Disclosures: May Fu: None; Xinyan Fu: *Employee*, Hangzhou Zhi-wei Information&Technology Ltd.; Hong Yuan: None; Guoping Zhang: None; Shihong Zhang: None; Xiangui Peng: None; Zhen Wang: None; Hongyang Zhang: None; Fengqi Fang: None; Xinyi Cao: *Employee*, Hangzhou Zhi-wei Information&Technology Ltd.; Mingyi Chen: *Advisory Board Member*, ALAB

Background: The myelodysplastic syndromes (MDS) comprise a heterogeneous group of malignant hematopoietic stem cell disorders characterized by ineffective hematopoiesis and increased risk of transformation to acute myeloid leukemia (AML). MDS exhibts morphological dysplasia and quantitative abnormality in the hematopoietic cells. The diagnosis of MDS depends on bone marrow aspirate smear 500-cell differential count to determine the percentage of blasts and dysplastic features. The morphological discrimination of bone marrow myeloblasts from promyelocytes, early erythroblasts and lymphoblasts can be challenging.

Design: In this study, we applied an automated marrow cell differential counting system (MorphGO) from bone marrow smear images using a dual-stage convolutional neural network (CNN) to help the diagnosis of MDS and AML. A systematic attempt was made to predict myeloblasts irrespective of the presence or absence of cytoplasmic granules using machine-learning techniques and artificial neural network. We performed the study in 25 cases of high grade MDS and 107 cases of AML. Multiple models were generated for each cell type with 100-500 training images. Internal accuracies and generalisation accuracies were compared. The uncertained classification of immature cells was further adjusted by pathologists. The data was correlated with the findings of immunophenotype by flow cytometry, cytogenetics and FISH results.

Results: We trained and tested our methods on a dataset of 26,346 immature cells using correlation and cross-validation techniques. The selected of 10,000 patch images of myeloblasts were collected for training. The dual-stage CNN classified images into myeloid, erythroid and lymphoid immature mononuclear cells, and achieved an accuracy of 95.5%, sensitivity of 73.5% and specificity of 97.5% in MDS cases. The proposed method not only showed high classification performance, but also successfully classified variant images without cytoplasmic granules by manual adjustable atypical features extracted by implementing CNN.

Figure 1 - 1808

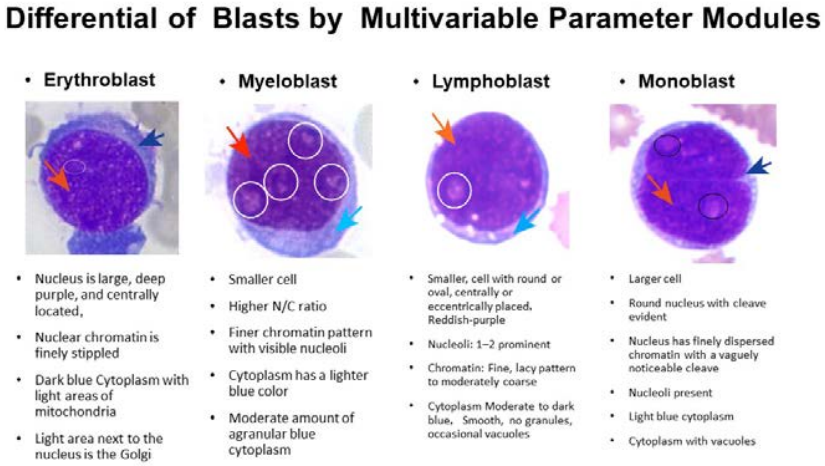

Conclusions: The MorphoGO machine learning based system is effective for classifying immature mononuclear cells in MDS/AML diagnosis. The percentage of blasts calculated by the AI system in the marrow smear is superior to those calculated by flow cytometry. This automatic system improves the consistency and diagnostic accuracy. This AI-based approach for evaluating MDS/AML highlights its viability as a powerful tool for best practices of hematopathology.

1809 Validation of EDTA Decalcification for Clinical Molecular Next Generation Sequencing (NGS) Studies

Filippo Galbo[1], Charlene Gettings[2], Rachel Poon[3], Kyle Parker[4], Rishikesh Haridas[1], Nicole Cipriani[3], Jeremy Segal[5]
[1]The University of Chicago Medicine, Chicago, IL, [2]American Association of Pathologists' Assistants (AAPA), St. Paul, MN, [3]The University of Chicago, Chicago, IL, [4]University of Chicago Medicine, Chicago, IL, [5]The University of Chicago, Riverside, IL

Disclosures: Filippo Galbo: None; Kyle Parker: None; Rishikesh Haridas: None; Nicole Cipriani: None

Background: As the clinical need for NGS grows, so does the need for high quality formalin-fixed paraffin embedded (FFPE) tissue specimens. Decalcification with harsh (formic or hydrochloric) acids can destroy nucleic acids, possibly delaying patient treatment and making for costly sample failures. Alternative EDTA chelation methods are more likely to maintain the integrity of nucleic acids for NGS studies. The aim of this study is to evaluate DNA quantity and quality following decalcification in EDTA solutions over varying strengths and lengths of time, in order to implement a standardized decalcification protocol for all calcified specimens encountered in the gross pathology laboratory.

Design: Tissue sections from tonsil and uterine leiomyoma were fixed in formalin, decalcified in 10% and 18% EDTA for 0, 1, 3, 7, 14, and 21 days, and processed routinely into FFPE blocks. Unstained slides were cut and DNA was extracted from 4 slides (Qiagen DNA Investigator) from each of the 24 samples. DNA quantity was measured by Qubit2.0 Fluorometer (ThermoFisher). DNA quantity and quality was assessed via qPCR (Kapa hgDNA Quantification and QC kit) run in quadruplicate with 129bp and 305bp primers. DNA quality was assessed via fragment analysis on the six 18% EDTA tumor specimens (TapeStation 2200, Roche).

Results: DNA quantity and quality was similar between samples across time points (Fig 1). All samples passed mass requirements (100 ng) for a large NGS assay, despite size variation between samples from days 0-7 versus 14-21. DNA quality of the six 18% EDTA tumor specimens remained adequate for sequencing across time points (Fig 2).

	Average Qubit (ng)	Qubit Standard Deviation	Average hgQuant (ng)	hgQuant Standard Deviation
Tonsil_10%	5600	703	1307	381
Tonsil_18%	5296	2481	1141	717
Tumor_10%	3751	1773	1316	698
Tumor_18%	1349	354	347	183

Figure 1 - 1809

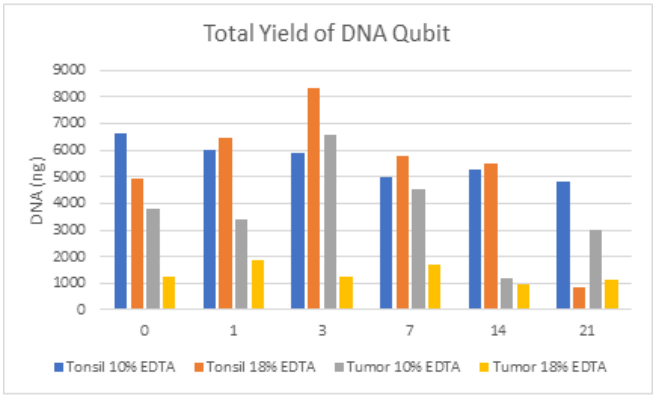

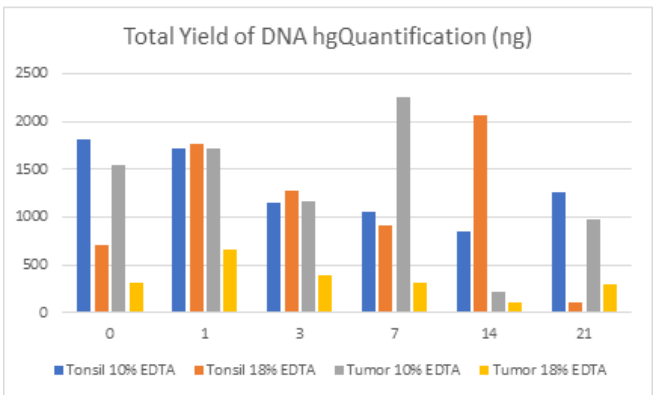

Figure 2 - 1809

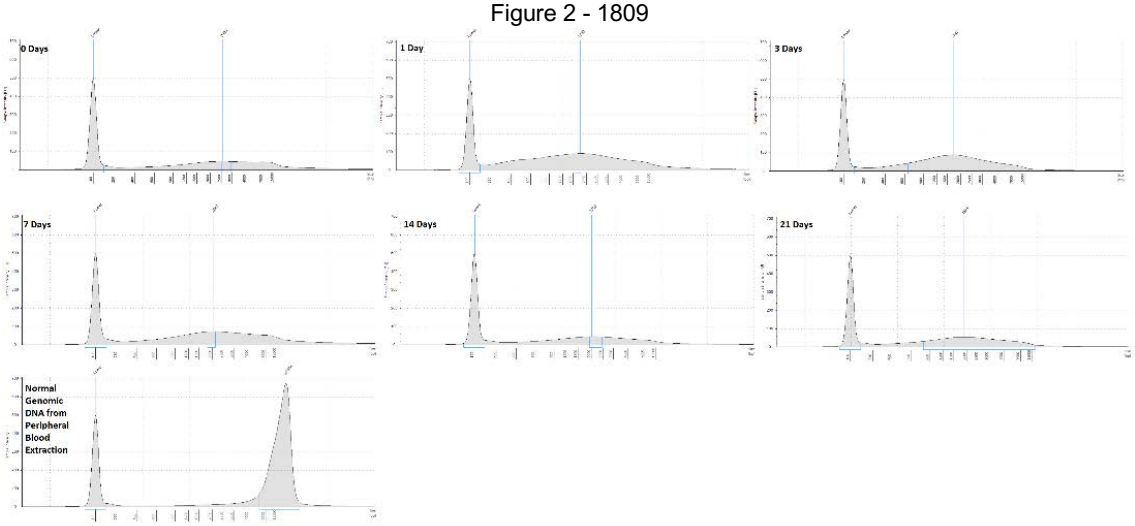

Conclusions: This study concludes that decalcification in 10% or 18% EDTA for up to 3 weeks gives sufficient high-quality genomic DNA for use in NGS assays. EDTA decalcification solutions are a preferable alternative to harsh acids in order to preserve nucleic acids, as evidenced here in both lymphoid and solid tumor specimens.

1810 Evaluation of the Tumor Microenvironment in Mycosis Fungoides using the NanoString PanCancer IO360TM Panel

Sharon Germans[1], Ozlem Kulak[2], Jesse Jaso[3]
[1]University of Texas Southwestern, Dallas, TX, [2]UT Southwestern Medical Center, Dallas, TX, [3]University of Texas Southwestern Medical Center, Dallas, TX

Disclosures: Sharon Germans: None; Ozlem Kulak: None; Jesse Jaso: None

Background: Mycosis fungoides (MF) is a cutaneous T-cell lymphoma with an indolent clinical course, but a subset of patients undergo disease progression and decreased survival. The cutaneous lesions of MF progress from “early-stage” lesions composed of flat patches and plaques to “late-stage” raised lesions.

Earlier studies showed an association between disease progression in MF and an immunosuppressed tumor microenvironment with activation of the PD-1/PD-L1 pathway. Chronic immunosuppression results in increased functional “exhaustion” of cytotoxic CD8(+) T-cells which are anergic to tumoral antigens.

The NanoString PanCancer IO 360™ panel uses 770 probes against genes, cells, and molecules associated with immunosuppression. The nCounter® platform converts raw counts from each probe to a $\log^2$ scale and normalizes the data against signals from 10 housekeeper (HK) genes to assign a “score” for each probe. A “tumor inflammation” score (TIS) is calculated that quantifies the magnitude of immunosuppression. A TIS of >5 has been shown to predict response to PD-1 blockade in solid tumors.

Design: The electronic medical record and H&E-stained punch biopsies were reviewed to select 4 early-stage MF lesions and 4 late-stage lesions. RNA was pooled from unstained formalin-fixed, paraffin-embedded (FFPE) tissue sections and analyzed on the nCounter® platform using the IO 360 ™ panel. An HK score was calculated for each sample to assess RNA integrity prior to analysis (minimum score of 5 required for analysis).

Results: The specimens had a mean HK score of 9 (range, 7.7-10.1) and a TIS of > 5 (median, 7.4, range 5.4 – 10.2). A heat map of gene signatures showed increased (>5) scores for several signatures involved in immunosuppression (Figure 1A-B). Late-stage lesions showed an increase in exhausted CD8 cells (p=0.02). Late stage lesions also showed higher scores for PD1 but results did not reach statistical significance (p= 0.15).

Figure 1 - 1810

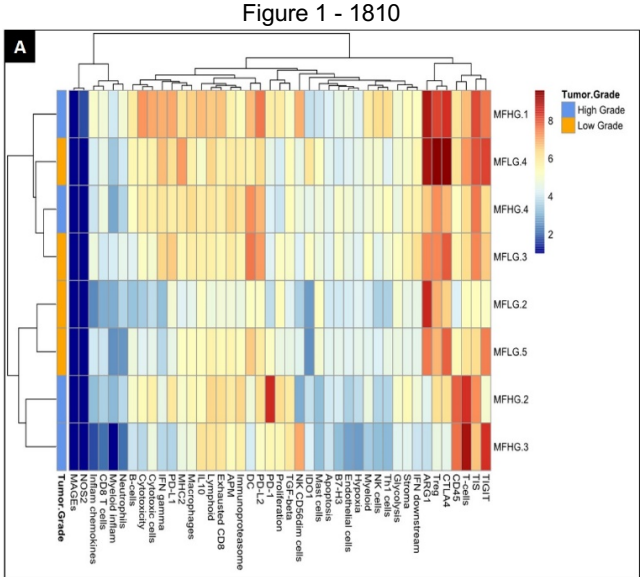

Figure 2 - 1810

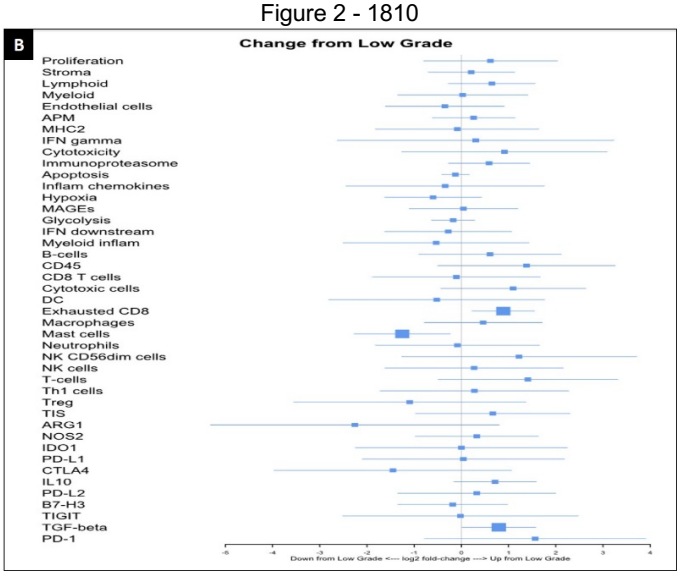

Conclusions: Our findings confirm that small punch biopsies contains sufficient RNA integrity for analysis on the NanoString platform. They also suggest the presence of an immunosuppressive microenvironment in MF, with a resultant increase in exhausted CD8(+) T-cells.

Our findings provide justification for a larger study of the microenvironment in MF using Nanostring. The Nanostring platform may be preferable to other methods due to its high sensitivity, lack of amplification errors, and ability to utilize small FFPE samples.

1811 Transposable Elements and the Tumor Immune Landscape in Human Cancer

Nicolas Giraldo-Castillo[1], Parnaz Daneshpajouhnejad[2], Daphne Wang[3], Markku Miettinen[4], Tricia Cottrell[5], Janis Taube[6], Avi Rosenberg[6], Kathleen Burns[6]
[1]Johns Hopkins Medical Institutions, Baltimore, MD, [2]Baltimore, MD, [3]Johns Hopkins Medicine, Baltimore, MD, [4]National Cancer Institute, Bethesda, MD, [5]Queen's University, Kingston, ON, [6]Johns Hopkins University School of Medicine, Baltimore, MD

Disclosures: Nicolas Giraldo-Castillo: None; Parnaz Daneshpajouhnejad: None; Daphne Wang: None; Markku Miettinen: None; Tricia Cottrell: None; Janis Taube: None; Avi Rosenberg: None; Kathleen Burns: *Primary Investigator*, EMD Millipore

Background: Nearly half of the human genome is made up of transposable element sequences, and there are more than 100 intact, protein-coding long interspersed element-1 (LINE-1) copies, capable of producing additional copies of themselves. Recent evidence suggests that LINE-1 expression is often dysregulated in cancer and that new insertions can cause driver and passenger mutations. This study aims to characterize the expression of LINE-1 in major types of human cancer, and correlate this expression with the tumor immune landscape and patient prognosis.

Design: Tissue microarrays (TMA) composed of n=480 specimens from 20 tumor types were stained for expression of LINE-1-encoded open reading frame 1 protein (ORF1p) by chromogenic IHC and visually scored. Two tumor types (lung and melanoma) were further characterized for this study. Specifically, additional TMAs composed of n=60 non-small cell lung cancer cases [n=30 squamous cell carcinoma (SCC) and n=30 adenocarcinomas (AC)] and n=93 melanoma specimens were also stained by multiplex immunofluorescence for CD8, CD163, FoxP3, PD1, PDL1, and a mix of tumor antigens (AE1/AE3 or Sox10/S100). Expression of ORF1p on tumor cells and the immune cell infiltrates was quantified using digital pathology or image cytometry platforms, respectively.

Results: LINE-1 ORF1p expression varied significantly across cancer type. Non-small cell lung cancer [SCC n=35/38 (92%) and AC n=32/38 (84%)], head and neck SCC [n=26/41 (63%)], and breast carcinoma [n=38/61 (62%)] showed the largest proportions of cases expressing ORF1p. In contrast, only a moderate fraction of melanomas expressed this protein [n=6/35 (17%)]. Other tumors (e.g., kidney cancer, GIST, rhabdomyosarcoma) showed low or no ORF1p expression. Preliminary analysis of the immune infiltrate in n=30 lung SCC showed that the expression of ORF1p on tumor cells positively correlates with the densities of CD8+ (p=0.05) and PDL1+ cells (p=0.03). Co-expression studies showed that two populations in particular (CD8+PD1+ T cells and non-tumor PDL1+ cells) were responsible for these associations.

Conclusions: These preliminary data underscore that the aberrant over-expression of LINE-1 ORF1p is heterogeneous across tumor types, and potentially associate LINE-1 with an immunoactive microenvironment. In the next phase of this project, in addition to investigating this correlation in larger cohorts of patients, we will explore how these associations relate to tumor mutational burden and clinical outcome.

1812 Light-Sheet Microscopy for 3D Pathology of a Variety of Human Tissues

Adam Glaser[1], Nicholas Reder[1], Lawrence True[2], Jonathan Liu[1]
[1]University of Washington, Seattle, WA, [2]University of Washington Medical Center, Seattle, WA

Disclosures: Adam Glaser: *Consultant*, LightSpeed Microscopy; Nicholas Reder: *Employee*, Lightspeed Microscopy, Inc.; Lawrence True: *Stock Ownership*, Lightspeed Microscopy, Inc.; Jonathan Liu: *Stock Ownership*, LightSpeed Microscopy Inc.

Background: In recent years, advances in tissue clearing and light-sheet microscopy have enabled unprecedented access to the structural and molecular contents of biological tissues. These techniques enable visualization of entire 3D specimens without the need to produce glass slides. However, previous systems and protocols have not been optimized for high-throughput clinical imaging, limiting their overall utility. Here we present an easy-to-use and non-destructive microscope, in conjunction with a tissue-clearing and labeling protocol that enables robust 3D pathology of a variety of human tissues.

Design: A custom-built open-top light-sheet (OTLS) microscope was used to image an array of human tissue types (normal and malignant), including prostate, breast, skin, lung, and bone. All datasets were reconstructed in 3D using custom software and the ImageJ plug-in BigStitcher. All tissues were cleared using a modified iDISCO protocol to make the specimens transparent for 3D imaging. They were stained using a fluorescent analog of H&E staining. In the case of bone, specimens were decalcified using EDTA prior to clearing and staining.

Results: The OTLS system was able to provide sub-micron resolution at an imaging speed of ~1 mm^3/min, with a maximum usable imaging depth of 0.5 cm and lateral area of 10×10 cm. The modified iDISCO protocol was able to successfully clear all specimens up to 5 mm in thickness within 2 days. Fluorescent staining over 1 day was able to penetrate the full volume of all specimens, revealing nuclear

and cytoplasmic structures at depth. The total size of each dataset ranged from 0.1 - 2.4 terabytes. Examination of the tissues in 3D revealed disease features which would not have been identified in conventional 2D sections.

Figure 1 - 1812

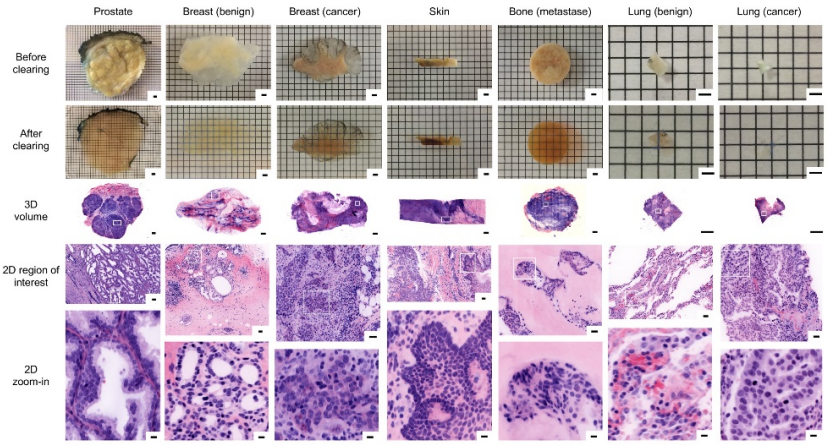

Conclusions: Our optimized clearing, labeling, and imaging protocols are able to produce 3D images of a variety of intact human tissues with a similar appearance to 2D H&E-stained tissue sections. In combination, these methods might transform histopathology practice by simplifying the pathology workflow, preserving tissues for downstream assays (through nondestructive imaging), and providing volumetric information with diagnostic benefits. Ongoing studies aim to demonstrate the benefits of 3D pathology for guiding treatment decisions.

1813 Millisect Automated Tissue Dissection: A Novel and Efficient Tool for Selected Tissue Sequencing

Charles Havnar[1], Oliver Zill[1], Ryan Jones[2], Justin Balko[3], Jennifer Giltnane[1], Carmina Espiritu[1], Jeff Eastham[1], Nicolas Lounsbury[1], Daniel Oreper[4], Suchit Jhunjhunwala[1], Katrina Krogh[5], Mahesh Yadav[1], Richard Bourgon[1], Guang-Yu Yang[2], Amy Lo[1]

[1]Genentech, Inc., South San Francisco, CA, [2]Northwestern University, Chicago, IL, [3]Vanderbilt University Medical Center, Nashville, TN, [4]Genentech, Inc., San Francisco, CA, [5]McGaw Medical Center of Northwestern University, Chicago, IL

Disclosures: Charles Havnar: None; Oliver Zill: *Employee*, Genentech; Ryan Jones: None; Justin Balko: None; Jennifer Giltnane: *Employee*, Genentech; Carmina Espiritu: None; Jeff Eastham: None; Nicolas Lounsbury: None; Daniel Oreper: *Consultant*, Genentech; Suchit Jhunjhunwala: None; Katrina Krogh: None; Mahesh Yadav: None; Richard Bourgon: *Employee*, Roche; *Stock Ownership*, Roche; Guang-Yu Yang: None; Amy Lo: *Stock Ownership*, Roche

Background: Whole exome sequencing (WES) provides valuable tumor mutation data, but results in loss of tissue context. Existing technologies such as macrodissection and laser capture microdissection (LCM) do not provide sufficient harvest precision or are time consuming and expensive. Therefore, we utilized the AVENIO Millisect (AM) system to test whether automated dissection (AD) with precision between macrodissection and LCM would allow us to select individual regions of interest (ROIs) from unstained FFPE sections for extraction and WES.

Design: FFPE tissues with confirmed high-quality nucleic acid were identified. Areas of interest were annotated on digital H&E images and overlay tissue masks were applied to adjacent levels of serially sectioned unstained slides. The AM AD system was utilized to harvest ROIs by on-slide tissue milling with mineral oil or nuclease free water pre- and post-deparaffinization. Nucleic acid extraction was performed with various kits or automated platforms and quantity and quality was measured prior to WES and downstream bioinformatics analysis.

Results: Hardware and software functionality improvements following identification of workflow challenges resulted in successful AD on FFPE sections up to 20mm. Various harvest fluids and deparaffinization procedures led to successful nucleic acid extraction, but greater DNA and RNA yield was detected following harvest from deparaffinized unstained slides. Improved RNA integrity was apparent when samples were harvested in mineral oil compared with nuclease free water. WES demonstrated significant correlations of both median coverage and variant allele frequency (VAF) with percent viable tumor, and separately of TMB, with percent tumor and proportion of necrotic tissue.

Conclusions: We demonstrate that the AM AD instrument for FFPE tissue harvest provides sufficient precision for mutation analysis without loss of tissue context in a fast and inexpensive fashion not offered by existing technologies. Deparaffinized samples harvested in mineral oil and extracted with the Promega Maxwell system provided the best nucleic acid yield without sacrificing quality while WES demonstrated correlation of coverage, VAF, and TMB with tumor viability. AM AD provides tumor enrichment for small ROIs as well as

regional comparisons from the same slide. The resulting mutational profiles with maintenance of tissue context could help inform basic science research, clinical trials, and patient care.

1814 Association of Inactivating ARID1A Variants and Tumor Mutation Burden

Magdalena Jurkiewicz[1], Wanying Zhang[2], Susan Hsiao[3], Mahesh Mansukhani[1], Helen Fernandes[4]
[1]Columbia University Medical Center, New York, NY, [2]White Plains, NY, [3]New York-Presbyterian/Columbia University Medical Center, Flushing, NY, [4]Columbia University, New York, NY

Disclosures: Magdalena Jurkiewicz: None; Susan Hsiao: None; Mahesh Mansukhani: *Speaker*, Promega; Helen Fernandes: None

Background: *ARID1A* (AT-rich interaction domain 1A) that encodes a SWI/SNF family member and functions in chromatin remodeling is often mutated in several cancer types. Most *ARID1A* variants are inactivating mutations leading to loss of ARID1A expression. *ARID1A* inactivation is reported to be associated with compromised MMR and increased mutagenesis. Furthermore, *ARID1A* deficiency is correlated with microsatellite instability (MSI) and increased Tumor Mutation Burden (TMB) across multiple human cancer types, suggesting that tumors that harbor *ARID1A* mutations may have a higher likelihood of response to PD-1 and PD-L1 targeted immunotherapy. Our aim was to assess the association between *ARID1A* mutation and TMB in a cohort of 154 patients with diverse cancer types.

Design: Pathology data and molecular results were collected from clinical reports generated using our in-house validated and New York State approved NGS panel. All cases were sequenced with a 467 gene hybrid capture NGS panel that covers 1.27 Mb of sequence. TMB per Mb was calculated from the number of nonsynonymous and indel variants identified in our patient cohort and reported as low (0-2.36 mutations/Mb), intermediate (2.37-3.94 mutations/Mb), or high (>3.95 mutations/Mb). Association between *ARID1A* mutation and TMB was evaluated using the Mann-Whitney U Test (SPSS). In order to understand biological pathways affected through mutations in tumor samples, we evaluated each tumor's mutational profile with Gene Set Enrichment Analysis (GSEA).

Results: Of 154 cases with varying tumor types, 76 were classified as "TMB Low," 49 as "TMB Intermediate" and 29 as "TMB High" according to the classification scheme described above. In the "TMB low" group, 3 cases harbored *ARID1A* mutations (3.9%), 2 of which are premature termination or frameshift mutations (2.6%). In the "TBM Intermediate" group, there were 5 cases with *ARID1A* mutations (10.2%), 4 of which are premature termination or frameshift mutations (8.2%) and in the "TMB High" group, there were 6 *ARID1A* mutations (20.7%), 4 of which are frameshift (13.8%). *ARID1A*-mutated cancers demonstrated a significantly higher TMB than *ARID1A*-wildtype cancers (Mann-Whitney U test, P= 0.01) (Figure 1).

Conclusions: Our results support prior studies that have shown that *ARID1A* mutated cancers demonstrate a significantly higher tumor burden. In the absence of known biomarkers, *ARID1A* could potentially be a surrogate marker for identification of tumors that would be more likely to respond to immunotherapy.

1815 Expression Analysis of Immune Modulatory Molecules HLA-E and HLA-F in 69 Cases of Glioblastoma: An Association with Survival

Leos Kren[1], František Siegl[2], Alena Kopkova[2], Jiri Sana[3], Zdenka Krenova[1]
[1]University Hospital Brno, Brno, Czech Republic, [2]CEITEC - Central European Institute of Technology, Masaryk University, Brno, Czech Republic, [3]Masaryk University, Brno, Czech Republic

Disclosures: Leos Kren: None; František Siegl: None; Alena Kopkova: None; Jiri Sana: None; Zdenka Krenova: None

Background: Glioblastoma (GB) is considered to be one of the deadliest human cancers, which responds poorly to both traditional and experimental therapeutic approaches, stubbornly persisting with a dismal survival of about 12–15 months from diagnosis. Central nervous system has been traditionally considered an immunologically privileged site; GB appears to benefit from this immunosuppressive milieu. Human leukocyte antigens E and F (HLA-E, HLA-F) are nonclassical HLA class I molecules well known to be involved in the protection of semi- allogeneic fetal allografts from the maternal immune system, and in transplant tolerance and viral and tumoral immune escape. The role of HLA-G and HLA-E expression in GBM is not well characterized.

Design: We performed qRT PCR analyses of the HLA-E and HLA-F expressions in 69 GB tissue samples and 21 non-tumor brain tissues (obtained from resections from drug-resistant epilepsy patients). GB patients underwent standard therapeutic protocol including surgical resection followed by the concomitant chemoradiotherapy with temozolomide. Total RNA from all tumor and brain non-tumor tissue specimens was extracted and further analyzed using specific TaqMan Gene Expression Assays (ThermoFisher Scientific). MGMT methylation status as well as IDH1 mutation status were evaluated in all GBs.

Results: Statistical analysis revealed that both HLA-E and HLA-F are significantly upregulated in GB samples in comparison with non-tumor brain tissues (Fold Change (FC) = 2.05, $p < 0.001$; and FC = 2.02, $p = 0.001$, respectively; Mann-Whitney analysis). Contraintuitively, subsequent survival analyses showed significant ($p = 0.01$; Kaplan-Meier analysis) association between low expression of HLA-E and

shorter overall survival (OS) of GB patients (median OS = 8.9 months vs. 13.5 months in patients with high HLA-E expression). Similar but not significant association has been observed also in HLA-F (p = 0.16). Finally, we showed that ionizing radiation (RT) increased both HLA-E and HLA-F expressions in GB cells in vitro in dose and time dependent manners.

Conclusions: We described deregulated expressions of HLA-E and HLA-F in GBM tissue in comparison with non-tumor brain tissue and showed that HLA-E could be a promising prognostic molecule in GBM patients; and suggested that nonclassical HLA class I molecules are affected by RT. This work was supported by Ministry of Health of the Czech Republic - grant No. 17-32758A; and by institutional funding of Faculty Hospital Brno.

1816 Analysis of microRNAs in 86 Samples of Cerebrospinal Fluid: A New Possible Diagnostic Tool in Brain Tumor Patients

Leos Kren[1], Zdenka Krenova[1], Alena Kopkova[2], Jiri Sana[3], Ondrej Slaby[3]
[1]University Hospital Brno, Brno, Czech Republic, [2]CEITEC - Central European Institute of Technology, Masaryk University, Brno, Czech Republic, [3]Masaryk University, Brno, Czech Republic

Disclosures: Leos Kren: None; Zdenka Krenova: None; Alena Kopkova: None; Jiri Sana: None; Ondrej Slaby: None

Background: Cerebrospinal fluid (CSF) may represent an ideal source of diagnostic biomarkers of brain tumors. MicroRNAs (miRNAs), short non-coding RNAs involved in the pathogenesis of many cancers including brain tumors, might represent group of new biomarkers. Analysis of CSF miRNAs in brain tumor patients may lead to new promising tools, both diagnostic and prognostic, enabling more precise brain tumor classification and future tailored therapy.

Design: Analysis of global miRNA profiles by next-generation sequencing (NGS) has been performed in 89 CSF samples obtained from 32 cases of glioblastomas (GB), 14 low-grade gliomas, 11 meningiomas and 13 brain metastasis patients and 19 non-tumor donors. 4 – 6 mL of CSF samples have been obtained during the lumbar puncture before surgical intervention in brain tumor patients or during standard therapy management of patients with normal-pressure hydrocephalus (non-tumor donors). CleanTag Small RNA Library Prep Kit were used for cDNA library preparation. NextSeq 500 instrument together with Next 500/550 High Output v2 Kit - 75 cycles were used for final sequencing analysis.

Results: NGS analysis revealed 22, 12, 35, and 11 CSF miRNAs with different levels in GB, meningiomas, brain metastases, and low-grade gliomas (adj.p < 0.0005, adj.p < 0.01 and adj.p < 0.005, p < 0.1) respectively, in comparison with non-tumor CSF samples. Levels of 9 miRNAs (let-7a, let-7b, miR-10a, miR-10b, miR-21-3p, miR-30e, miR-140, miR-196a and miR-196b) were validated in independent set of CSF samples (41 GBM, 8 low-grade gliomas, 44 meningiomas, 12 metastasis patients and 21 non-tumor donors) using TaqMan Advanced miRNA Assays. We successfully validated all selected miRNAs identified by NGS to have significantly (adj. p < 0.05) different levels in CSF of GB. In case of meningioma we confirmed 2 out of 5 miRNAs and in brain metastasis 2 out of 6 miRNAs were independently validated. We also successfully validated 5 out 6 miRNAs in low-grade gliomas. we also show miR-10b and miR-196b in CSF to be potential prognostic biomarkers in GB patients.

Conclusions: We showed significant differences in CSF miRNA levels in patients with various brain tumors. Our results suggest potential of CSF miRNAs to be useful biomarkers in brain tumors. This work was supported by Ministry of Health of the Czech Republic - grants nr. 15-34553A and 17-32758A; and by institutional funding of Faculty Hospital Brno.

1817 Prognosis-Informed Phenotype Assignment (PIPA): A Novel Method for Unsupervised Discovery of Cell Phenotypes with Prognostic Significance in the Tumor Microenvironment

Mai Chan Lau[1], Juha Väyrynen[2], Melissa Zhao[1], Sara Väyrynen[2], Simeng Gu[1], Koichiro Haruki[1], Jonathan Nowak[1], Shuji Ogino[1]
[1]Brigham and Women's Hospital, Boston, MA, [2]Dana-Farber Cancer Institute, Boston, MA

Disclosures: Mai Chan Lau: None; Juha Väyrynen: None; Melissa Zhao: None; Sara Väyrynen: None; Simeng Gu: None; Koichiro Haruki: None; Jonathan Nowak: None; Shuji Ogino: None

Background: Multiplex imaging assays can rapidly generate histologic data with single-cell resolution. However, cell phenotype assignment can be challenging, as most existing methods rely upon explicitly defined combinatorial marker intensity cutoffs. We hypothesized that tumor prognostic information could be leveraged to identify novel cell phenotypes that are jointly defined by protein expression and morphology and that may provide new insights into tumor biology.

Design: Prognosis-informed Phenotype Assignment (PIPA) is a computational approach that discovers cell phenotypes based upon phenotypic features that best distinguish tumors with different prognoses. These features are used to build a phenotyping model using unsupervised clustering on a subset of the cells of interest. This model that can then be applied to the entire data set using a k-Nearest Neighbor classifier to phenotype all cells of interest. As a proof of principle, PIPA was employed to discover macrophage phenotypes in

931 colorectal cancers (CRCs) using a multiplexed immunofluorescent panel (CD68-CD86-IRF5-MRC1-MAF-CK-DAPI) designed for measuring macrophage polarization and density.

Results: PIPA identified nine distinct macrophage phenotypes across 931 CRCs. High densities of two phenotypes were significantly associated with longer cancer-specific survival (CSS) (log-rank $p \leq 0.001$ for both). One phenotype remained significant after adjustment for microsatellite instability status, stage, and tumor differentiation using a Cox proportional hazards model ($p < 0.001$ for intraepithelial density). This macrophage phenotype was characterized by variable cell size and shape and modest expression levels of polarization markers, while the other prognostically favorable phenotype was characterized by high expression of M1 marker CD86 and high nuclear and membrane roundness. Conversely, high intraepithelial density of another phenotype, showing high expression of M2 marker MRC1 and high cytoplasmic compactness, was associated with worse CSS ($p = 0.007$).

Conclusions: PIPA offers a novel method for cell phenotype discovery that uses a combination of protein expression, cell morphology and prognostic information. In a large CRC cohort, this unsupervised approach identified prognostically relevant cell phenotypes that overlap but also expand upon previously described phenotypes, such as M1 and M2-type macrophages. PIPA is expected to be applicable across tumor types for phenotyping a wide variety of cells.

1818 Clinical Validation of Low-Voltage "Compact" Transmission Electron Microscopy for Ultrastructural Evaluation of Kidney and Heart Biopsy Samples

Rebecca Lawrence[1], Jorge Isaac[1], Isaac Lloyd[2], Dylan Miller[3]
[1]Intermountain Medical Center, Salt Lake City, UT, [2]Utah Pathology Services, Inc., Bluffdale, UT, [3]Intermountain Central Lab, Salt Lake City, UT

Disclosures: Jorge Isaac: None; Isaac Lloyd: None; Dylan Miller: None

Background: Transmission electron microscope (TEM) use remains an integral part of the pathologic evaluation of renal biopsies, certain cardiac biopsies, and various other specimen types. TEM instruments and cameras are costly, occupy a substantial floor space footprint, and are associated with significant overhead costs (maintenance contracts and power requirements for the microscope, vacuum pumps, cooling system, and computers). Compact TEM instruments that operate at 25 kEV (compared to 80-120 kEV for conventional TEMs) have recently become available. They use an ordinary power outlet, and occupy a comparatively small footprint with all components self-contained. We report the results of a clinical validation exercise using a parallel testing approach; comparing the diagnostic utility of images obtained on a conventional TEM and compact TEM.

Design: 90 consecutive clinical biopsies and 10 pre-selected biopsies known to have certain ultrastructural features of interest were selected for parallel testing. These included 85 native kidney, 5 transplant kidney, and 10 heart biopsies; from 99 patients. The samples were prepared for TEM examination per routine protocols (including osmium post-fixation and uranyl acetate – lead citrate staining of grid sections). The samples were examined using a JEOL 1010 TEM at 80 kEV using a Veleta side-mount 4MP camera and the iTEM imaging interface (Olympus) and also using a DeLong Instruments LVEM25 benchtop TEM at 25 kEV using its 5.5MP camera and included digital imaging interface. Three pathologists captured images of the specimens in the course of their routine clinical work. Images were later retrospectively compiled and reviewed for salient ultrastructural features in a systematic fashion. Comparisons were made between the images and diagnostic findings obtained from each camera.

Results: No discrepancies were seen in the ability of the compact TEM instrument to resolve any of the findings seen using the conventional TEM instrument. There were qualitative differences in the image appearance, as expected, but these did not substantially limit the diagnostic interpretation of these 100 cases. Some representative comparisons of ultrastructural findings with each instrument are shown in [FIGURE 1]

Figure 1 - 1818

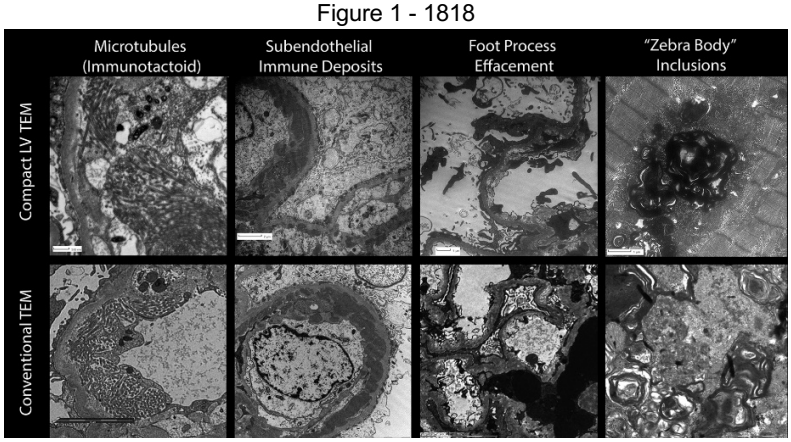

Conclusions: Compact TEM is a clinically valid means of ultrastructural evaluation of renal and cardiac biopsy specimens with a comparable ability to discriminate key diagnostic findings in these samples.

1819 Comparison of Different Monoclonal Antibodies for Detection of Programmed Cell Death Ligand 1 (PD-L1) in Breast, Colorectal and Liver Carcinomas

Zaibo Li[1], Konstantin Shilo[2], Christina Hopkins[2], William Joy[3], Andrew Margerrison[4], Keith Wharton[5], Anil Parwani[2]
[1]The Ohio State University Wexner Medical Center, Columbus, OH, [2]The Ohio State University, Columbus, OH, [3]Leica Biosystems, Danvers, MA, [4]Leica Biosystems, Newcastle, Tyne and Wear, United Kingdom, [5]Leica Biosystems, Rockport, MA

Disclosures: Zaibo Li: None; Konstantin Shilo: None; Christina Hopkins: None; William Joy: None; Andrew Margerrison: *Employee*, Leica Biosystems; Keith Wharton: *Employee*, Leica Biosystems; *Consultant*, Novartis AG; Anil Parwani: None

Background: Several antibodies targeting PD-L1 are in clinical use as diagnostic tests for cancer immunotherapies, including 22C3 and 28-8 (Dako/Agilent), and SP263 (Roche/Ventana). The objective of this study was to evaluate different commercially available PD-L1 clones with a novel clone 73-10 (Leica Biosystems), shown in BLUEPRINT2 to be the most sensitive among these clones in lung carcinomas.

Design: FFPE Tissue Micro Arrays (TMA) constructed from 208 breast carcinomas, 208 hepatocellular carcinomas and 208 colorectal carcinomas were assessed by immunohistochemistry (IHC) using monoclonal antibodies 73-10 (BOND-III, Leica Biosystems), SP263 (BenchMark ULTRA, Roche/Ventana), 22C3 and 28-8 (Autostainer Link 48 stainer, Dako/Agilent). The IHC expression on tumor cells (TC) and immune cells (IC) was interpreted by board certified pathologists (Figure 1: Representative images of PD-L1 expression in breast cancer using 73-10, SP263, 22C3 and 28-8), and pairwise agreement of positivity at >1% cells between assays/platforms were determined.

Results: Across all tested tissues, the percent of PD-L1 positive cases was the highest with SP263 on both TC (13% in breast, 5.9% in liver, 3.4% in colorectal) and IC (16% in breast, 26% in liver, 51% in colorectal). Other clones scored as follows: 22C3 (TC: 9.8% in breast, 3.4% in liver, 1.5% in colorectal; IC: 7.4% in breast, 8.8% in liver, 28% in colorectal), 28-8 (TC: 11% in breast, 3.9% in liver, 2.5% in colorectal; IC: 8.8% in breast, 17% in liver, 24% in colorectal) and 73-10 (TC: 11% in breast, 4.4% in liver, 3.1% in colorectal; IC: 12% in breast, 15% in liver, 29% in colorectal). Clone 73-10 demonstrated substantial agreement (k >0.61) with other clones SP263, 22C3 and 28-8 for assessment of TC in all tested tissues, with near perfect agreement observed (k >0.81) with 22C3, 28-8 and SP263 in breast cancer tissues and with 28-8 and 22C3 in liver cancer tissue.

	73-10	SP263	28-8	22C3
Breast cancer				
73-10	X	0.81	0.98	0.89
SP263	0.81	X	0.79	0.71
28-8	0.98	0.79	X	0.92
22C3	0.89	0.71	0.92	x
Liver cancer				
73-10	X	0.75	0.82	0.87
SP263	0.75	X	0.69	0.72
28-8	0.82	0.69	X	0.79
22C3	0.87	0.72	0.79	X
Colorectal cancer				
73-10	X	0.83	0.72	0.66
SP263	0.83	X	0.66	0.59
28-8	0.72	0.66	X	0.75
22C3	0.66	0.59	0.75	X

Table 1: *k* agreement among different PD-L1 clones in breast, liver and colorectal carcinoma tumor cells

Figure 1 - 1819

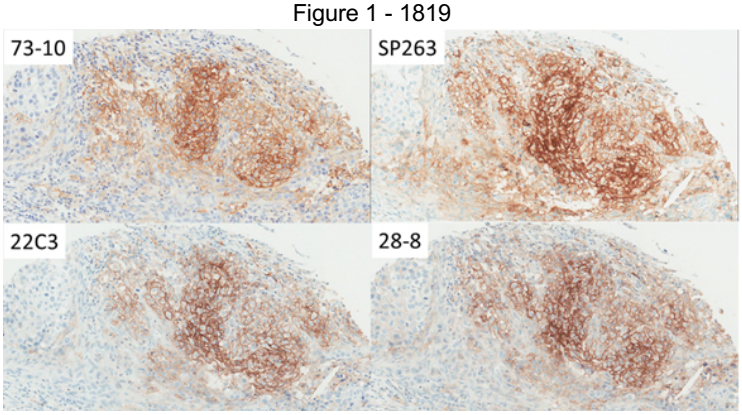

Conclusions: Our data indicates that the four clones tested demonstrate largely comparable PD-L1 expression on tumor cells. In our TMA cohorts, SP263 was the most sensitive clone for PD-L1 detection on tumor and immune cells in breast, liver and colorectal cancers. The observed difference between our results and the BLUEPRINT2 study of lung cancers that showed 73-10 as the most sensitive of the antibodies tested might be tissue-, platform-, and/or protocol-specific, and warrants further investigation.

1820 Powerful Multi-Region Sequencing and Somatic Mutation Clonality Analysis of Intratumoral Heterogeneity on Paired Primary and Metastatic Tumor Samples

Amy Lo[1], Charles Havnar[1], Ryan Jones[2], Carmina Espiritu[1], Jeffrey Eastham[1], Nicolas Lounsbury[1], Daniel Oreper[3], Suchit Jhunjhunwala[1], Katrina Krogh[4], Mahesh Yadav[1], Richard Bourgon[1], Guang-Yu Yang[2], Oliver Zill[1]
[1]Genentech, Inc., South San Francisco, CA, [2]Northwestern University, Chicago, IL, [3]Genentech, Inc., San Francisco, CA, [4]McGaw Medical Center of Northwestern University, Chicago, IL

Disclosures: Amy Lo: *Stock Ownership*, Roche; Charles Havnar: None; Ryan Jones: None; Carmina Espiritu: None; Jeffrey Eastham: None; Nicolas Lounsbury: None; Daniel Oreper: *Consultant*, Genentech; Suchit Jhunjhunwala: None; Katrina Krogh: None; Mahesh Yadav: *Employee*, Genentech; Richard Bourgon: *Employee*, Roche; *Stock Ownership*, Roche; Guang-Yu Yang: None; Oliver Zill: *Employee*, Genentech

Background: Significant gaps in understanding intratumoral heterogeneity (ITH) exist, particularly in advanced or pre-treated tumors, despite increased efforts to characterize tumor evolution and selective pressures. We therefore performed multi-region sequencing (MR-seq) and somatic mutation clonality analysis to determine how mutation clonality varies between regions within and between primary and metastases in the same patient. We additionally sought to determine how predictive single tissue blocks are for assessing clonality in metastatic tumors.

Design: The MR-seq literature was reviewed to identify number of patients with both primary and metastatic regions sequenced across several solid tumor indications. Patients with at least 3 regions (>1cm apart) from a primary, 3 regions from regional metastasis, 3 regions of distant metastasis and paired normal at a single surgical timepoint were identified from two advanced colorectal carcinomas (CRC), one

renal cell carcinoma (RCC), one urothelial carcinoma and one non-small cell lung carcinoma (NSCLC). AVENIO Millisect automated dissection for tumor enrichment was performed on tumor regions from unstained FFPE slides and whole exome sequencing and somatic-mutation and copy-number-alteration analyses (CNA) were performed.

Results: Literature review revealed no MR-seq literature on head and neck squamous cell carcinoma as well as limited MR-seq data (>2 regions per patient) in all metastatic indications. MR-seq of NSCLC and urothelial carcinoma cases suggested more clonal patterns across primary and metastatic regions, with the CRC and RCC cases appearing more heterogenous. Analysis of CNA enabled identification of tumor regions with poor tumor content or sample quality, helping us to calibrate somatic mutation detection across tumor regions. Multi-region analysis of individual metastases identified distinct early- or late-branching metastases across different cases.

Conclusions: Significant gaps exist in the MR-seq literature, and we have generated MR-seq data across metastatic indications to elucidate global mutation clonality in this setting. ITH varied between cases and indications, and these differences may impact recommended tumor sampling approaches. Determining whether certain sites (primary, metastasis or both) are best evaluated to assess a single patient will provide important information to help guide therapy development for patients in aggressive disease settings with limited treatment options.

1821 Development of Novel Monoclonal Antibodies for the Robust Detection of CD28, CD80 and CD86 by Immunohistochemistry in Human Tumors

Gary Means[1], Russell Sanderson[1], Brian Johnson[2], Megan Larmore[3], Mark Maurer[1], Stanford Peng[1]
[1]Alpine Immune Sciences, Seattle, WA, [2]University of Washington, Seattle, WA, [3]Northwestern University, Chicago, IL

Disclosures: Gary Means: *Employee*, Alpine Immune Sciences; *Stock Ownership*, Alpine Immune Sciences; Russell Sanderson: None; Brian Johnson: None; Megan Larmore: None; Mark Maurer: *Employee*, Alpine Immune Sciences, Inc.; Stanford Peng: *Employee*, Alpine Immune Sciences

Background: The CD28-CD80/CD86 costimulatory pathway plays a critical role in T cell activation and is implicated in the prognosis of cancers and in their response to immunotherapies. Expression of CD28, CD80, and/or CD86 may therefore serve as clinically significant prognostic biomarkers. However, no validated reagents are currently available for the assessment of these targets by immunohistochemistry (IHC). The present effort was undertaken to identify and to develop robust IHC reagents for these targets, in part to enable a diagnostic assay for our novel immuno-oncology drug candidate, ALPN-202, a conditional CD28 co-stimulator and dual PD-L1/CTLA-4 checkpoint inhibitor in an upcoming phase 1 clinical trial.

Design: Commercially available monoclonal antibodies (mAb) reported to detect CD28, CD80 or CD86 by IHC were evaluated in FFPE tonsil, thymus and cerebellum using multiple antigen retrieval conditions. Proprietary mouse and rabbit mAbs directed against CD28, CD80 and CD86- identified during hybridoma campaigns and selected via ELISA, western blot, and flow cytometry- were similarly assessed for suitability in IHC. Target reactive mAbs were further evaluated using a range of tumor sections and tumor microarrays (628 individual samples). IHC results were compared to mRNA expression as assessed by PCR on duplicate slides.

Results: Eight mAbs (two commercial, six proprietary) demonstrated IHC staining in thymus and tonsil with sufficient sensitivity and precision to advance to evaluation in tumor sections and microarrays. At least one proprietary mAb specific for each target, respectively, was identified and demonstrated robust staining across multiple tissues with excellent inter-reader precision. Representative mAb IHC images of GALT are shown below (Figure 1). RNA expression generally correlated with IHC, particularly in regions of high specificity such as lymphoid organs. Full results, including correlations with RNA expression and accuracy/specificity across tumor arrays, will be presented.

Figure 1 - 1821

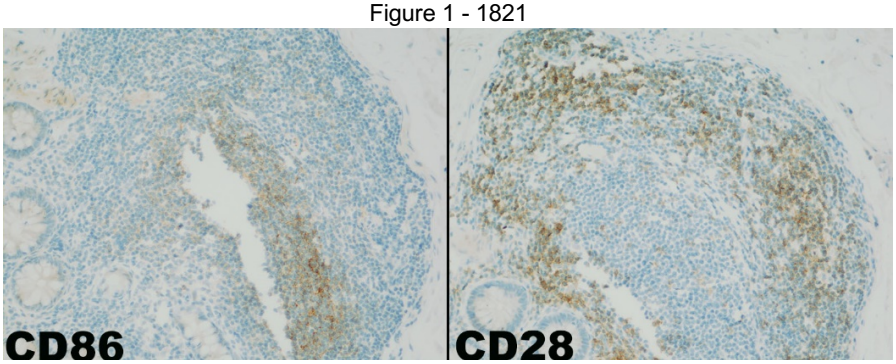

Conclusions: Successful development of proprietary mAb against CD28, CD80, and CD86 has been accomplished with good performance characteristics in IHC applications. Such reagents will be particularly useful in future studies to assess the prognostic

relevance of these biomarkers in cancer and other diseases; and also- may be incorporated in companion diagnostic strategies for patient stratification in trials of drugs involving checkpoint inhibition and/or T cell co-stimulation.

1822 To Diagnose Intestinalization, Orcein-Alcian Blue is an Easier, Faster and Possibly More Beneficial Alternative to PAS-Alcian Blue

Jeremy Minkowitz[1], Christopher Shutty[2], Gerald Minkowitz[2], George Serobian[3]
[1]NYIT-COM, Brooklyn, NY, [2]Minkowitz Pathology, Brooklyn, NY, [3]Fordham University

Disclosures: Jeremy Minkowitz: None; Christopher Shutty: None; Gerald Minkowitz: None

Background: Gastroesophageal reflux disease (GERD) plagues millions of Americans with symptoms that are uncomfortable and that can transform into intestinal metaplasia or adenocarcinoma. Monitoring patients with chronic GERD is routine. Standard sampling requires a tissue biopsy of the gastroesophageal junction. Hematoxylin and Eosin staining is most commonly used to interpret these specimens. Intestinal metaplasia is characteristically associated with sialomucin secreting glandular epithelium. Cells that produce sialomucin have a better prognostic outcome than sulfonated mucins (sulfomucins). Orcein stains positive for sulfomucins and may be used as a counterstain. Staining with Alcian Blue (AB) can easily identify sialomucin formations and Periodic Acid Schiff (PAS) or Nuclear Fast Red (NFR) is typically its counterstain. These staining techniques are time consuming. One PAS-AB protocol can take up to 30 minutes to process which contributes to costly technician time and unproductive use of bench space. We suggest that by implementing a simplified rapid microwavable Orcein-Alcian Blue (AB) stain, suspected metaplastic regions can be more quickly and accurately identified. This more efficient testing protocol frees up valuable resources. The effectiveness of the Orcein-AB stain in identifying intestinal metaplasia utilizes its full potential to stain for sulfomucins, a possible biological marker of adenocarcinoma.

Design: Fifty cases with known esophageal metaplasia were identified between 2018 and 2019. Forty gastric and lower intestinal biopsies were identified for negative and positive controls. These biopsies were bathed in 2% acetic orcein and microwaved for 5 minutes at 55°C with agitation. The specimens were then washed in 1% Acetic Acid and were subsequently rinsed in tap water. They were then stained with alcian alue for 1 minute and were rinsed in tap water again. The results were compared with a standard NFR-Alcian Blue protocol.

Results: Our results demonstrate that Orcein-AB differentiates intestinal sialomucin producing cells from typical gastric type mucin producing cells in the upper gastrointestinal tract as accurately and in less time than PAS-AB.

Conclusions: Historically, Orcein-AB protocols were long and labor intensive. PAS-AB stains were originally faster. Our novel rapid technique levels the playing field with orcein being effectively implemented in the determination of intestinal metaplasia. Many other potential uses for this protocol are anticipated in the future.

1823 Next-Generation Protocols for Tumor Organoid Development in Precision Oncology

Kentaro Ohara[1], Maria Laura Martin[2], Wael Al Zoughbi[3], Anastasia Tsomides[1], Cynthia Cheung[1], Adriana Irizarry[2], Phoebe Reuben[2], Olivier Elemento[4], Juan Miguel Mosquera[1], Rema Rao[5]
[1]Weill Cornell Medicine, New York, NY, [2]Englander Institute for Precision Medicine, New York, NY, [3]Weill Cornell Medicine, New York City, NY, [4]New York, NY, [5]New York-Presbyterian/Weill Cornell Medical Center, New York, NY

Disclosures: Kentaro Ohara: None; Maria Laura Martin: None; Wael Al Zoughbi: None; Anastasia Tsomides: None; Cynthia Cheung: None; Adriana Irizarry: None; Phoebe Reuben: None; Olivier Elemento: None; Juan Miguel Mosquera: None; Rema Rao: None

Background: Development of patient-derived tumor organoids is a promising preclinical model in precision care because they recapitulate the genomic and phenotypic features of original tumors. However, culturing organoids has several drawbacks: it is costly, time-consuming and has the risk of benign cell 'contamination'. We integrated Cytopathology assessment into our precision medicine workflow to ensure successful organoid development towards molecular characterization, high-throughput drug screening and potential co-clinical trials.

Design: Fresh tissue biopsies and resection specimens were procured by Surgical Pathology. After cytopathology smear confirmation of 'donor' tumor, samples were processed for organoid cultures. Successful cultures showed viable cells forming spheroid-like structures and propagated for at least five passages (P5). Further evaluation of organoids at P3 and/or P5 were performed using smears and cellblocks. Ancillary studies including immunohistochemistry, molecular characterization with whole exome sequencing (WES), RNA-seq and drug screening were performed on successful cultures.

Results: 386 samples from 342 patients (190 biopsies, 174 resection specimens, 15 ascites and 7 blood clots) from 17 organ systems and 15 tumor types, were procured for organoid cultures (Table). 63 specimens (16.3%) showed successful cultures and additional 13 (3.4%) are currently in P3. 29 cases (7.5%) failed to grow due to contamination of bacteria or yeast. Benign overgrowth was observed in 25 cultures (6.5%). Organoid development from biopsies was less successful (11.6%) than that from ascitic fluid (33.3%) and resections (20.1%). Organoid development from colorectum (30%), esophagus/stomach (27.3%) and ovary/fallopian tube (26.7%) was more

successful than those from prostate (9.7%), breast (9.7%) and pancreas (10.5%). In successful cultures, the cytomorphology between organoids and native tumors showed good concordance (Figure 1). WES profiles of sequenced organoids and those of matched tumors showed fair concordance in the somatic mutations (median, 62.5%; range 8.3 - 100).

Established organoids based on specimen and tumor types					
Tumor Type	**Biopsy**	**Resection**	**Clot**	**Ascites**	**Total**
Adenocarcinoma	14/138	25/97	1/7	5/13	45/255
Renal cell carcinoma	2/11	2/21	0/0	0/0	4/32
Urothelial carcinoma	0/11	4/20	0/0	0/0	4/31
Ductal carcinoma	2/13	1/16	0/0	0/0	3/29
Sarcoma	0/4	0/2	0/0	0/2	0/8
Carcinoma, NOS	0/4	0/2	0/0	0/0	0/6
Small cell carcinoma	3/5	1/1	0/0	0/0	4/6
Squamous cell carcinoma	1/1	0/4	0/0	0/0	1/5
Carcinosarcoma	0/1	0/3	0/0	0/0	0/4
Benign*	0/0	1/3	0/0	0/0	1/3
Neuroendocrine tumor	0/1	0/2	0/0	0/0	0/3
Mucinous borderline tumor	0/0	1/1	0/0	0/0	1/1
Lymphoma	0/0	0/1	0/0	0/0	0/1
Lobular carcinoma	0/1	0/0	0/0	0/0	0/1
Sex cord stromal tumor	0/0	0/1	0/0	0/0	0/1
Total	22/190	35/174	1/7	5/15	63/386
*Renal angiomyolipoma, renal oncocytoma and thyroid adenomatous nodule					

Figure 1 - 1823

Figure 2 - 1823

Figure 1

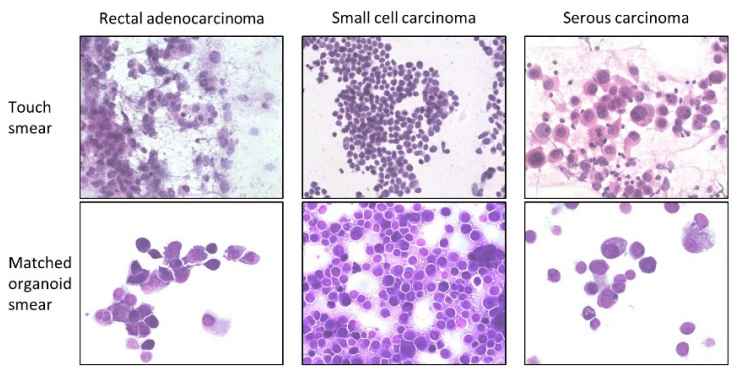

Figure 2. Organoid development workflow

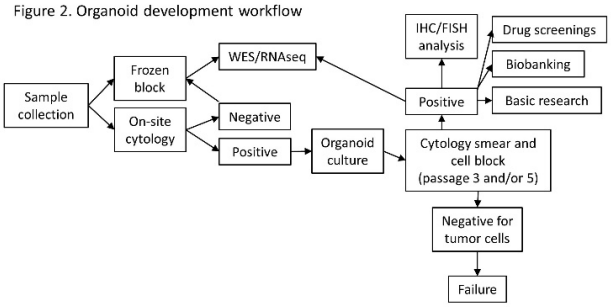

Conclusions: We established an organoid development workflow that incorporates cytopathology during tissue triaging and organoid evaluation (Figure 2). Cytopathology plays a key role to improve the efficiency of tumor organoid cultures, aiming to guide precision care of cancer patients.

1824 3D Morphology Using CHiMP System Multiphoton Microscopy is Equivalent to Light Microscopy to Report Liver Biopsies

Pallavi Patil[1], Richard Torres[2], Dhanpat Jain[1], Romulo Celli[3]
[1]Yale University School of Medicine, New Haven, CT, [2]Yale School of Medicine, New Haven, CT, [3]Guilford, CT

Disclosures: Pallavi Patil: None; Richard Torres: *Stock Ownership*, Applikate Technologies, LLC; Dhanpat Jain: None; Romulo Celli: None

Background: Traditional histology light microscopy (LM) processing is the current standard for generating pathologic diagnoses; however, is time and labor intensive, and is prone to processing errors. Most slide free methods have limitations like slow speed, superficial tissue scanning and suboptimal images. The Clearing Histology with Multiphoton Microscopy (CH*i*MP) system has previously shown to overcome these limitations, particularly in the analysis of prostate biopsies. Liver biopsies, which have a complex set of parameters to analyze and often require timely interpretation, may be amenable to CH*i*MP.

Design: Core biopsies were obtained from excess tissue from liver resection specimens. Processing involved alcohol-based dehydration incorporating nuclear and protein fluorescent dyes, followed by dehydration in high refractive index fluid over 2 hours. Samples were placed in rectangular fluid-filled chambers and imaged on a prototype fast multiphoton microscope at 250 nm lateral resolution and two-channel fluorescence digitally converted using CH*i*MP, and subsequently processed for LM. H&E slides and CH*i*MP images were independently evaluated by two pathologists with a 3-week washout period between two methods. Ancillary stains routinely used for liver biopsy were not included for analysis. Time to diagnosis, fibrosis score (based on H&E only), and diagnosis were evaluated.

Results: Nine core biopsies were included. CH*i*MP provided equivalent image quality to LM and visualization of the entire core on the Macro view. There were no differences in the diagnoses generated by CH*i*MP and LM. There was one major discrepancy in the evaluation of fibrosis in which CH*i*MP identified cirrhosis and by LM there was only focal bridging fibrosis seen (Figure 2). The time to arrive at a diagnostic interpretation was longer for CH*i*MP than LM (user 1: average 1 min 53 sec for CH*i*MP vs 1 min 25 sec for LM, and user 2: average 1 min 43 sec for CH*i*MP vs 47 sec for LM); however, five image stacks were evaluated on CH*i*MP images, and only one LM level was evaluated.

Case	Diagnosis	Discrepancy
1	Liver with mild portal inflammation and bile ductular reaction	
2	Adenocarcinoma, favor metastatic colon	
3	Hemangioma	
4	Cirrhotic liver with marked inflammation and bile ductular reaction	Fibrosis score 4 on Ch*i*MP vs focal fibrosis score 2 on light microscopy
5	Cirrhotic liver moderate septal inflammation	
6	Near normal liver biopsy with minimal steatosis	
7	Adenocarcinoma, favor metastatic colon	
8	Near normal	
9	Near normal	Fibrosis grade score 0 to 1 on CH*i*MP and score 1 to 2 on light microscopy

Figure 1 - 1824

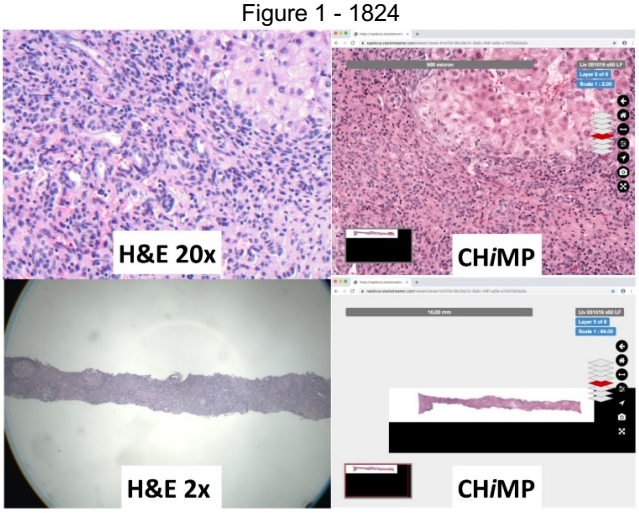

Figure 2 - 1824

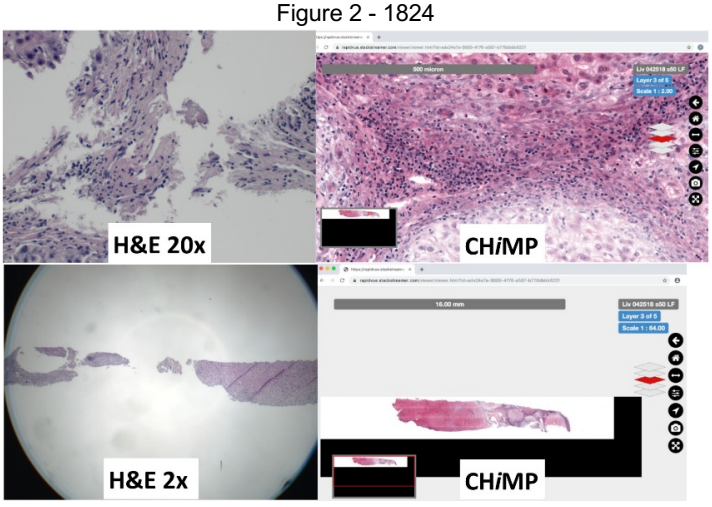

Conclusions: The analysis of liver biopsies using CH*i*MP demonstrated equivalent and potentially superior material for diagnoses generation. CH*i*MP presents several advantages compared to other slide-free and LM methods, including shorter time of image acquisition, deeper tissue imaging, no loss of tissue and lower cost. Evaluation of a high throughput slide-free clinical workflow is required for future use.

1825 Clinical Validation of a Fluorescence In Situ Hybridization (FISH) Approach for Homozygous CDKN2A/MTAP Deletion

Lauren Ritterhouse[1], Ryan Frazier[2], Jochen Lennerz[1]
[1]Massachusetts General Hospital, Harvard Medical School, Boston, MA, [2]Massachusetts General Hospital, Boston, MA

Disclosures: Lauren Ritterhouse: None; Ryan Frazier: None; Jochen Lennerz: None

Background: *CDKN2A is a tumor suppressor gene and loss of the gene is often seen in the setting of homozygous deletion of the 9p21 locus. The locus includes CDKN2A/B and MTAP and is lost in ~15% of all human cancers. Homozygouys loss has diagnostic, prognostic, and potential predictive utilities; however, the practical approach on how to assess homozygous CDKN2A/MTAP loss in the clinical setting has to our knowledge not been reported.*

Design: To clinically validate the *CDKN2A* FISH assay for homozygous deletion, we tested using a commercial *CDKN2A* FISH probe at 9p21 (Abbott #05J51-001) covering a ~222 kb region that includes both *CDKN2A* and *MTAP* and a commercial centromere 9 probe at 9p11-9q11 (Abbott #05J51-001). FISH scoring was performed using combinatorial probe:CEP bins with enumeration of at least 50 nuclei. A sample is classified as positive for homozygous deletion if ≥10% of nuclei can be assigned to the definitive probe:CEP bin [ISCN: nuc ish (CDKN2A x0, CEP9 x2)]. Validation samples were identified from known samples with *CDKN2A* loss as determined by our laboratory developed NGS genotyping assay SNAPSHOT-NGS. We validated the information system-based reporting logic using synthetic datasets.

Results: FISH probe specificity was determined by analyzing the probe localization in 5 metaphase cells in which the *CDKN2A* probe hybridized to the 9p21.3 locus in 5/5 cells. Concordance of FISH with NGS, assessed using a total of 21 FFPE samples, was 100%; out of the 10 cases that were found to be negative for *CDKN2A* deletion by NGS, 10 were also negative by the FISH assay (10/10 = 100% negative agreement). A representative FISH image for a sample positive for CDKN2A homozygous deletion is shown in the Figure. Reproducibility was determined using replicate testing of 3 samples (2 positive, 1 negative) with 100% concordance across runs. Synthetic data confirmed accurate FISH scoring and ISCN reporting logic.

Figure 1 - 1825

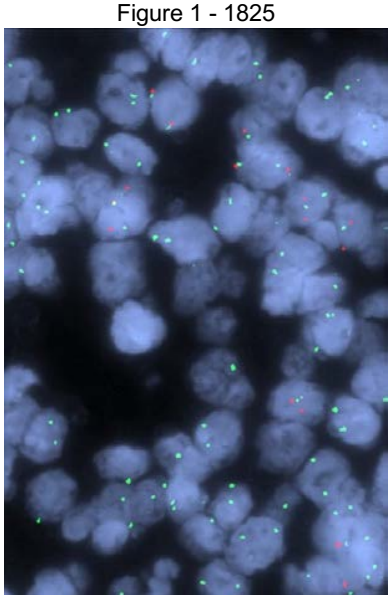

Conclusions: Although homozygous loss of *CDKN2A/MTAP* is a frequently identified molecular signature, the practical aspects of assessment on interphase FISH can be challenging due to a variety of signal patterns from both homozygous and hemizygous loss states, as well as amplification and monosomy. We demonstrate a practical approach for clinical validation using FISH with acceptable performance measures for testing in routine clinical practice.

1826 The Emerging Anti-Cancer Target KRAS G12C: A Pangenomic Study

Jeffrey Ross[1], Ethan Sokol[2], Russell Madison[2], Jon Chung[2], Vincent Miller[2], Siraj Ali[3], Julia Elvin[2], Jo-Anne Vergilio[2], Keith Killian[2], Douglas Lin[2], Erik Williams[4], Natalie Danziger[5], James Haberberger[6], Julie Tse[4], Shakti Ramkissoon[6], Eric Severson[6], Amanda Hemmerich[6], Naomi Lynn Ferguson[6], Claire Edgerly[6], Daniel Duncan[6], Richard Huang[7], Alexa Schrock[2]
[1]Upstate Medical University, Syracuse, NY, [2]Foundation Medicine, Inc., Cambridge, MA, [3]Cambridge, MA, [4]Boston, MA, [5]Foundation Medicine, Inc., Somerville, MA, [6]Foundation Medicine, Inc., Morrisville, NC, [7]Foundation Medicine, Inc., Cary, NC

Disclosures: Jeffrey Ross: *Employee*, Foundation Medicine; Ethan Sokol: *Employee*, Foundation Medicine; *Stock Ownership*, Roche; Russell Madison: *Employee*, Foundation Medicine Inc.; *Stock Ownership*, Roche; Jon Chung: *Employee*, Foundation Medicine; *Stock Ownership*, Roche; Vincent Miller: *Employee*, Foundation Medicine, Inc / Roche; *Stock Ownership*, Foundation Medicine / Roche; *Advisory Board Member*, Revolution Medicines; *Advisory Board Member*, Revolution Medicines; Siraj Ali: *Employee*, Foundation Medicine; *Advisory Board Member*, Incysus Therapeutics; *Consultant*, Takeda; Julia Elvin: *Employee*, Foundation Medicine; *Employee*, Hoffman La Roche; Jo-Anne Vergilio: *Employee*, Foundation Medicine, Inc; *Employee*, Foundation Medicine, Inc; Keith Killian: *Employee*, FMI; Douglas Lin: *Employee*, Foundation Medicine; Erik Williams: *Stock Ownership*, F. Hoffman-La Roche, Ltd.; *Employee*, Foundation Medicine, Inc.; Natalie Danziger: *Employee*, Foundation Medicine Incorporated; James Haberberger: *Employee*, Foundation Medicine Inc.; Julie Tse: *Employee*, Foundation Medicine, Inc.; *Consultant*, Pathology Watch, LLC.; Shakti Ramkissoon: *Employee*, Foundation Medicine/Roche; Eric Severson: *Employee*, Foundation Medicine; Amanda Hemmerich: *Employee*, Foundation Medicine, Inc; Naomi Lynn Ferguson: *Employee*, Foundation Medicine; Claire Edgerly: *Employee*, Foundation Medicine, Inc.; Daniel Duncan: *Employee*, Foundation Medicine; Richard Huang: *Employee*, Roche/Foundation Medicine; Alexa Schrock: *Employee*, Foundation Medicine; *Stock Ownership*, Roche

Background: *KRAS*, the most frequently activated oncogene in human cancer, has long been considered un-targetable. Recently, a specific short variant (SV) *KRAS* genomic alteration (GA), *KRAS* G12C, has emerged as an anticancer target with two recent major presentations demonstrating significant efficacy of novel kinase inhibitors in a variety of cancer types.

Design: Comprehensive genomic profiling (CGP) was performed on FFPE samples from 255,008 clinically advanced solid tumors and hematologic malignancies. Tumor mutational burden (TMB) was determined on 0.8 to 1.2 Mbp of sequenced DNA and microsatellite instability (MSI) was determined on 114 loci. PD-L1 expression in tumor cells (Dako 22C3) was measured by IHC.

Results: *KRAS* GA were identified in 59,770 (21.8%) of the 274,694 cases in which 8,278 (13.8%) were *KRAS* G12C. NSCLC, CRC and Pancreas accounted for 71% of all *KRAS* mutated cancers. In the 8,278 (3.0%) cases of *KRAS* G12C mutated cancers NSCLC, CRC and Pancreas accounted for 84% with NSCLC significantly contributing more cases than CRC and Pancreas (Table). The age and gender distributions were similar in all groups. The *TP53* and *CDKN2A/B* GA frequencies were similar in all groups with the *APC* GA lower in the *KRAS* G12C group ($p<0.001$). Biomarkers predicting an increased chance of immune checkpoint inhibitor (ICPI) response including TMB and PD-L1 expression were significantly greater in the *KRAS* G12C group. The *STK11* GA frequency associated with ICPI resistance was also significantly elevated in the *KRAS* G12C group when compared to all other *KRAS* mutations ($p<0.001$).

	KRAS only G12C mut			*KRAS* no G12C mut			*KRAS* All mut		
Total Cases	8,278			51,492			59,770		
Age (median + range)	65 (0-89+)			63 (0-89+)			63 (0-89+)		
Gender	M 43% F 57%			M 48% F 52%			M 47% F 53%		
Disease Prevalence (% of mutation type/% of disease type)	NSCLC	68%	11%	NSCLC	18%	19%	NSCLC	25%	30%
	CRC	13%	4%	CRC	27%	47%	CRC	26%	50%
	Pancreas	3%	2%	Pancreas	23%	82%	Pancreas	20%	84%
	Upper GI	0%	0%	Upper GI	2%	20%	Upper GI	2%	20%
	CUP	6%	4%	CUP	6%	21%	CUP	6%	24%
	Ovary	1%	1%	Ovary	3%	13%	Ovary	3%	13%
	Breast	1%	<1%	Breast	2%	4%	Breast	2%	4%
Other Gene Frequencies	*TP53*	53%		*TP53*	62%		*TP53*	61%	
	CDKN2A	24%		*APC*	26%		*CDKN2A*	25%	
	STK11	21%		*CDKN2A*	25%		*APC*	24%	
	CDKN2B	15%		*SMAD4*	14%		*CDKN2B*	14%	
	APC	14%		*CDKN2B*	13%		*SMAD4*	13%	
	RBM10	9%		*PIK3CA*	13%		*PIK3CA*	12%	
	PIK3CA	9%		*ARID1A*	8%		*STK11*	8%	
	ATM	8%		*MYC*	7%		*ARID1A*	8%	
	ARID1A	8%		*STK11*	6%		*MYC*	7%	
	MYC	7%		*PTEN*	6%		*PTEN*	5%	
	NKX2-1	7%		*FBXW7*	5%		*ATM*	5%	
	KEAP1	7%		*ATM*	5%		*FBXW7*	5%	
	LRP1B	7%		*GNAS*	5%		*GNAS*	5%	
	NFKBIA	6%							
	SMARCA4	6%							
	SMAD4	6%							
	DNMT3A	5%							
Cases MSI assessable	7420 (90%)			46200 (90%)			53620 (90%)		
MSI High Status	0.6%			2.2%			2.0%		
Cases TMB assessable	8265 (99.9%)			51430 (99.9%)			59695 (99.9%)		
Median TMB	7.0			3.5			3.5		
TMB> 10 mut/Mb	35.0%			12.1%			15.3%		
TMB> 20 mut/Mb	8.8%			4.4%			5.0%		
Cases PD-L1 assessable	1947 (23.5%)			7349 (14.3%)			9296 (51.6%)		
PD-L1 Low	22.9%			19.1%			19.9%		
PD-L1 High	37.5%			15.2%			19.9%		

Conclusions: *KRAS* G12C GA have different cancer type associations, GAs and biomarkers predicting responsiveness to non-KRAS targeted therapies and ICPI treatments. Given the recent successes of two anti *KRAS* G12C drugs in early clinical trials (Amgen AMG510; Miratti MRTX849), further study of the distribution, co-mutations potentially impacting drug response and potential for combination trials with ICPI in *KRAS* G12C altered malignancies appears warranted.

1827 Immune Contexture Quantification Using In Situ Single-Cell Multiplex Targeted Proteomic (ISSMART) Analysis: Method Development and Validation

Garazi Serna[1], Roberta Fasani[1], Laia Paré[2], Tomás Pascual[3], Xavier Guardia[1], Paqui Gallego[1], Gaia Griguolo[4], Jordi Canes[5], Antonio Llombart-Bosch[6], Javier Cortes[1], Patricia Villagrasa[7], Aleix Prat[8], Paolo Nuciforo[1]
[1]Vall d'Hebron Institute of Oncology, Barcelona, Spain, [2]Translational Genomics and Targeted Therapeutics in Solid Tumors Lab, Barcelona, Spain, [3]Hospital Clinic de Barcelona, Barcelona, Spain, [4]Istituto Oncologico Veneto IOV - IRCCS, Padova, Veneto, Italy, [5]SOLTI Breast Cancer Research Group,, Barcelona, Spain, [6]Universidad de Valencia, Valencia, Spain, [7]SOLTI Breast Cancer Research Group, Barcelona, Spain, [8]Hospital Clinic, Barcelona, Spain

Disclosures: Garazi Serna: None; Roberta Fasani: None; Laia Paré: None; Tomás Pascual: None; Xavier Guardia: None; Paqui Gallego: None; Gaia Griguolo: None; Jordi Canes: None; Antonio Llombart-Bosch: None; Javier Cortes: None; Patricia Villagrasa: None; Aleix Prat: None; Paolo Nuciforo: None

Background: Despite the remarkable success of cancer immunotherapies, the intrinsic complexity of the interaction between tumor and immune cells poses significant challenges on clinical response prediction. Novel multiplexed imaging techniques, which enable spatial cellular phenotyping of many markers at the same time on a single formalin-fixed, paraffin-embedded section, hold promise to interrogate more comprehensively cancer immunity thus providing valuable information for improving cancer immunotherapies. However, their widespread use is limited either by the complexity of the methodology or the need for expensive equipment.

Design: We developed a custom 6-plex panel for T cells immune contexture characterization including composition (CD3, CD4, CD8, FOXP3), localization (keratin for tumor recognition), and function (Ki67 for activity) using a novel immunohistochemistry (IHC) workflow called *IS*SMART which relies on sequential staining of multiple protein biomarkers on the same slide, virtual multiplexing, and digital image analysis. The methodology was validated in HER2-positive breast cancer core biopsies (baseline and day-15) from the SOLTI-PAMELA neoadjuvant trial. The primary objective was to correlate T cells densities (positive cells/mm^2) as determined by *IS*SMART with levels of stromal tumor-infiltrating lymphocytes (sTILs) determined by standard H&E assessment. Secondary objectives included correlation of immune contexture features with intrinsic subtyping as determined by PAM50 and pathologic complete response (pCR) following dual anti-HER blockade without chemotherapy.

Results: A total of 120 samples (66 baseline and 54 day-15) from 76 patients had residual material for *IS*SMART analysis (50% of recruited patients). In the entire cohort, the median (interquartile range) densities of CD3, CD8, CD4, and FOXP3 were 653(977.9), 144.4(350.5), 626.4(1203.7) and 162.6(251.3), respectively. Level of sTILs positively correlated with CD3 (Spearman rho, 0.65) and CD8 (0.56) densities (p<.0001 for both events). A significant increase from baseline to day-15 was observed for CD8 (median, 78.2 vs 207.6) and sTILs (10% vs 20%) (Kruskal-Wallis, p=0.04 for both events). Results of secondary objectives analyses will be presented.

Conclusions: We developed an innovative, automatized, sequential IHC workflow and analysis pipeline which allows for simultaneous imaging of several individual markers at single-cell resolution while preserving the intuitive visual output of traditional bright-field IHC.

1828 A Quantitative Chromogenic Technique for Imprinted Gene In Situ Hybridization (IGISH) - A New Addition for Enhanced Accuracy in Presurgical Diagnosis of Thyroid Cancers

Rulong Shen[1], Tong Cheng[2], Xing Li[2], Hongyu Yu[3], Yun Zhu[4], Hongxun Wu[5], Yifeng Zhang[6], Yun Liu[2], Jiandong Bao[5], Huixiong Xu[6], Ning Zhou[2]
[1]The Ohio State University Wexner Medical Center, Columbus, OH, [2]Epigentics Laboratory, Chinese Alliance Against Lung Cancer, Wuxi, Jiangsu, China, [3]Changzheng Hospital, China, [4]Jiangsu Institution of Nuclear Medicine, Wuxi, Jiangsu, China, [5]JiangYuan Hospital Affiliated to Jiangsu Institute of Nuclear Medicine, Wuxi, Jiangsu, China, [6]Shanghai Tenth People's Hospital, Ultrasound Research and Education Institute, Tongji University School of Medicine, Shanghai, China

Disclosures: Rulong Shen: *Advisory Board Member*, Lisen Imprinting Diagnostics, Inc.; Yun Zhu: None

Background: Thyroid nodules are common and are mostly benign. Ultrasound and even invasive FNA cytology have relatively low accuracies. Genetic biomarkers (e.g. BRAF, TERT) used as rule out tests reduce unneeded surgeries. Epigenetic changes, including Imprinted genes, often occur in early cancers (Feinberg AP. NEJM 2018;378:1323), but role in cancer diagnosis has been limited. Normal silencing of one of two parental alleles of Imprinted Genes is reportedly reversed in carcinogenesis, with expression of biallelic (Loss of Imprinting-LOI) or Multiallelic expression (Copy Number Variations-CNV). We present here a novel quantitative and chromogenic assay of imprinted genes LOI and CNV for detection of thyroid cancer.

Design: Chromogenic Imprinted gene in-situ hybridization (IGISH) technique uses RNAscope 2.5 HD assay kit with signal amplification and detection using chromogenic reagent Fast Red (ACD) (Fig 1). Probes targeting intron sequences of nascent RNAs visualizes the transcription sites, provides a quantitative analysis of the expression status of an imprinted genes panel (GNAS, GRB10 & SNRPN). A statistical diagnostic model based on LOI, CNV and Total Expression (TE) values is generated from 116 thyroid samples (79 malignant, 37 benign). The model was then validated in 181 presurgical FNA samples by comparing the prospective imprinting classification with cytopathology and follow up surgical histology.

Results: In the prospective validation cohort, IGISH detected 138 positive from 139 Papillary thyroid cancers (PTC) and identified as benign 39 of 42 benign samples (sensitivity of 99.3% and specificity of 92.9%). In contrast, only 87 (62.6%) PTC samples were detected as malignant by cytopathology and 50 (36.0%) were suspicious.(Fig 2) In addition, the sensitivity of BRAF V600E mutation was related to the cytopathological classification but IGISH was an independent classifier. There was 1 case with benign cytopathology and negative BRAF mutation, but was found highly positive by IGISH, that was proven PTC by surgery. These results indicate that IGISH is more sensitive than any currently used techniques and has no indeterminate zone.

Figure 1 - 1828

Fig 1. Different expression status of imprinted genes.

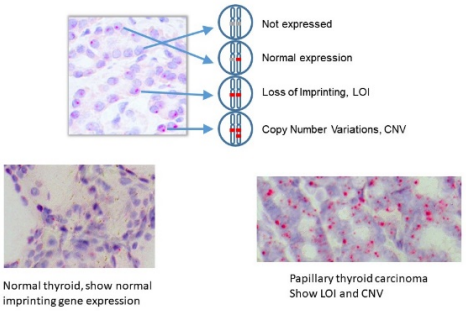

Figure 2 - 1828

Fig 2. Comparison of the sensitivities between cytopathology, BRAF, and imprinting detection.

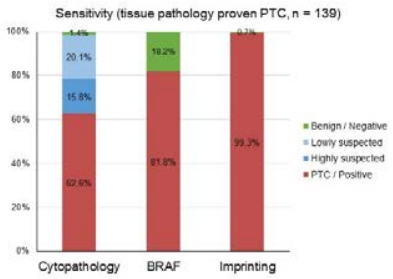

Conclusions: Our IGISH provides a novel way to visualize and quantify epigenetic changes in imprinting genes occurring in early thyroid cancers and can be a valuable adjunctive test to improve the accuracy of FNA cytopathology. Clinical application of this approach may reduce unneeded surgeries and reduce the cost for patients.

1829 Non-Destructive Chemical Imaging of Bone Tissue for Intraoperative and Diagnostic Applications

Kseniya Shin[1], Shuaiqian Men[1], Eleanor Chen[1], Dan Fu[1]
[1]University of Washington, Seattle, WA

Disclosures: Kseniya Shin: None; Shuaiqian Men: None; Eleanor Chen: None; Dan Fu: None

Background: Intraoperative consultations for bone tumors are challenged by inconclusive cytological preparations, while the high mineral and fat content of a specimen can severely compromise the quality of cryosectioned samples. Subsequent histological studies of these samples can be difficult to interpret as non-neoplastic collagenous stroma and neoplastic osteoid matrix can have a similar appearance, and histology offers scarce information about chemical changes in bone and osteoid matrix. Meanwhile, radiographic and spectroscopic studies of bone pathology show that there is abundant information available in both the mineral content as well as the collagenous matrix. In this study, we employ non-linear optical techniques including stimulated Raman scattering (SRS) and second harmonic generation (SHG) microscopy to provide unprecedented visualization of pathological processes reflected in the bone organic matrix and the mineral content.

Design: Tissue samples from 3 archival patient cases (1 normal and 2 osteosarcomas) were imaged using SRS and SHG microscopy (Fig. 1). Data in CH-region of the Raman spectrum provided protein chemical signature, and the morphology of tissue was visualized. The information in the fingerprint region of the Raman spectrum determined the carbonate substitution of hydroxyapatite (HAP). Collecting SHG signal, the quality of collagen was studied with particular attention to collagen fibril organization including basketweave, lamellar, and amorphous patterns. Finally, Amide I region was used to probe the spectral signature of the collagenous ma

Results: SRS data revealed that the carbonate content of HAP in osteoid produced by osteosarcoma was significantly lower than that of normal bone (Fig.2). Moreover, we found that SHG data demonstrated an expected mix of lamellar and basketweave pattern for the collagen fibril network in normal bone tissue. In contrast, SHG for the osteoid matrix in osteosarcoma showed frequently amorphous or minimally organized distribution pattern. Finally, the Amide I region data has demonstrated spectral differences between normal bone and neoplastic osteoid.

Figure 1 - 1829

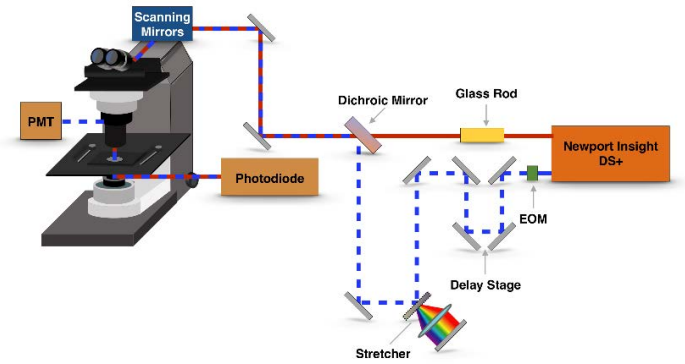

Figure 1: Schematic of SRS and SHG experimental setup.

Figure 2 - 1829

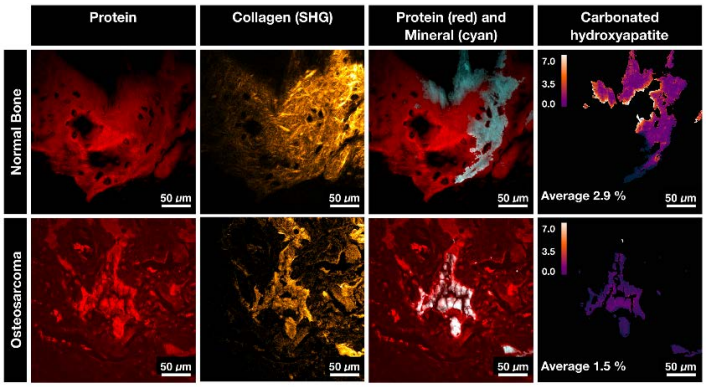

Figure 2: Comparison of SRS and SHG data for normal bone and neoplastic osteoid.

Conclusions: Our preliminary data demonstrates the feasibility of using a non-destructive method to image bone tissue with an unprecedented level of chemical and morphological detail. The observed differences in HAP, collagen distribution, and collagen spectrum when comparing between normal bone and osteosarcoma-produced osteoid demonstrate the promise for applications in pathology.

1830 Real-World Evidence of Temporal Variation in PD-L1 Expression

Sucha Sudarsanam[1], Medina Hatooglu[1], Dennis O'Malley[2], Lawrence Weiss[3]
[1]NeoGenomics Laboratories, Inc., Aliso Viejo, CA, [2]NeoGenomics Laboratories, Inc., Dana Point, CA, [3]NeoGenomics Laboratories, Inc., Pasadena, CA

Disclosures: Medina Hatooglu: None; Dennis O'Malley: None

Background: PD-L1 expression has become an important tool in assessing tumors for possible therapy with checkpoint immune regulation drugs. We evaluated PD-L1 expression changes in paired samples assessed at different times from the same patient.

Design: We analyzed paired specimens from 2,744 patients using PD-L1 22C3 antibody. We analyzed Tumor Proportion Score (TPS) collected at time T1 and T2, where T2 >= T1. Collection time of pairs varied between 0 (same day) and 360 days, with a median of 26 days. TPS was analyzed both as continuous and discrete variables. TPS was classified in two ways as follows: {0% NEGATIVE, >=1% POSITIVE} and {0% NOT EXPRESSED, >= 1% and <50% EXPRESSED, >50% HIGH EXPRESSION}. Variation was assessed using Wilcoxon and McNemar's tests.

Results: For pairs of specimens collected within 30 days, TPS at time T1 and time T2 do not vary significantly. For pairs of specimens collected more than 30 days apart, TPS at time T2 is greater than TPS at time T1 when TPS is treated as a continuous variable (p-value <= 0.026) (Image 1). For both the discrete cases, we also find that TPS at T1 and T2 have different proportions for time intervals greater than 30 days (<= 0.012 for {NEGATIVE, POSITIVE} and <= 0.037 for {NOT EXPRESSED, EXPRESSED, HIGH EXPRESSION}).

Figure 1 - 1830

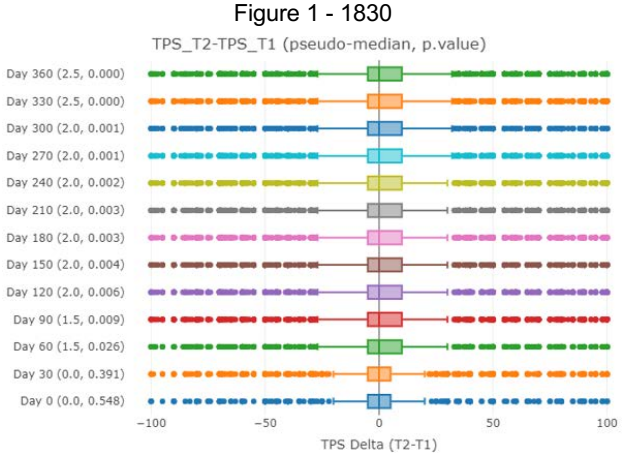

Conclusions: A variety of potential causes may underlie variation in PD-L1 scores with >30 day intervals between testing. Possibilities may include therapy effects, tumor evolution, or changes in immune regulation. Clinical information will be obtained to assess these potential causes.

1831 The Spectrum of Mixed Epithelial Stromal Tumors of the Kidney: A Histological, Ultrastructural, and Immuhistochemical Analysis of Four Cases, with Emphasis on Their Ovarian-Like Stroma

Ghita Tagmouti[1], Nuria Juanpere-Rodero[2], Beatriz Casado[1], Lluís Cecchini[2], Marta Lorenzo[2], Monica Gonzalez Farre[1], Belen Lloveras[1], Josep Lloreta-Trull[3]
[1]Hospital del Mar, Barcelona, Spain, [2]Hospital del Mar-Parc de Salut Mar-IMIM, Barcelona, Spain, [3]Hospital del Mar, Parc de Salut Mar, Universitat Pompeu Fabra, Barcelona, Spain

Disclosures: Ghita Tagmouti: None; Nuria Juanpere-Rodero: None; Beatriz Casado: None; Lluís Cecchini: None; Marta Lorenzo: None; Monica Gonzalez Farre: None; Belen Lloveras: None; Josep Lloreta-Trull: None

Background: Mixed epithelial and stromal tumors of the kidney (MESTK) are a subset of mostly benign neoplasms with epithelial and stromal components, the latter mimicking ovarian stroma. Interestingly, this finding is often seen in polycystic kidneys, among other non-neoplastic diseases. There is relatively little information on the morphology and the biological meaning of these lesions. This is a descriptive study of the light and electron microscopy (EM) features of four of these tumors, with particular emphasis in their stroma component.

Design: Four cases from the files of the 'Hospital del Mar' (PSMAR Biobanc) are the subject of this study. For comparison of the ovarian like stroma, we have included five cases each of autosomal dominant polycystic kidney disease (ADPKD), acquired cystic kidney disease (ACKD), xanthogranulomatous pyelonephritis (XP), and renal lithiasis (RL). In addition, we have included eight fetal, and five adult normal kidneys. A systematic study was performed of different cell compartments by transmission EM in the MESTK cases, as well as in one case in each of the other groups (FEI- Philips transmission electron microscope Hillsboro, Oregon, USA). Immunocytochemistry for Estrogen (ER) and Progesterone receptors (PR) was performed in all cases.

Results: By light and EM, all MESTK had a characteristic biphasic pattern. The stroma was monotonous in all cases. It consisted of spindle cells, containing variable amounts of non-membrane bound, moderately electron dense lipids, some mitochondria, as well as SER and RER. The epithelial component showed usually a tubular or microcystic arrangement, with microvilli and junctional complexes, abundant mitochondria and RER, but no lipid nor SER. ER and PR were expressed by stromal cells in all the cases, but not by the epithelial cells. Similar results were found in the cases of ADPKD, ACKD, XP and RL. The adult kidney controls were negative for ER and PR, but PR expression was found in half of the fetal controls.

Conclusions: MESTK tumors are not only biphasic, but they are amphicrine proliferations with exocrine epithelial and steroid secreting stromal components. Ultrastructural examination is essential in identifying this peculiar phenotype. The ovarian-like stroma in non-neoplastic kidney diseases has the same light and EM features. There is a transient phase with a similar phenotype in fetal kidneys of the second trimester. This finding suggests that MESTK could represent a neoplastic recapitulation of renal embryogenesis.

1832 Genetic Predisposition to High Interleukin-10 Production Protects from Allo-immune Response Related Complications of Transplantation

Gaurav Tripathi[1], Rehan Faridi[2], Khadeeja Tariq[3], Poonam Khan[2], Noureddine Berka, Victor Lewis[4], Jan Storek[3], Faisal Khan[2]
[1]University of Calgary, Calgary, AB, [2]Cumming School of Medicine, University of Calgary and Division of Hematopathology, Alberta Public Laboratories, Calgary, AB, [3]Cumming School of Medicine, University of Calgary, Calgary, AB, [4]Alberta Children's Hospital, Calgary, AB

Disclosures: Gaurav Tripathi: None; Rehan Faridi: None; Khadeeja Tariq: None; Poonam Khan: None; Noureddine Berka: None; Victor Lewis: None; Jan Storek: None; Faisal Khan: None

Background: Allo-immune responses after transplantation lead to severe complications like graft versus host disease (GVHD) after allogeneic Hematopoietic Cell Transplantation (HCT) and renal allograft failure after kidney transplantation. Cytokines act as chief mediators/regulators of allo-immune responses. Genetic control of cytokine production is evidenced by polymorphisms in cytokine gene regulatory regions resulting in low, moderate, or high cytokine production. Here, we investigated cytokine gene variants in two independent cohorts of allogeneic HCT donor-recipient pairs and recipients of kidney transplantation to assess their impact on the incidence of GVHD after HCT and renal allograft failures after kidney transplantation.

Design: A total of 864 subjects including 323 first allogeneic HCT donor-recipient pairs and 218 renal transplant recipients were recruited. The analysis was performed for 22 single nucleotide variants located in the regulatory and/or exonic regions of 13 cytokine/cytokine receptor genes using PCR-SSP approach. The panel of genes includes *TNF-a*, *IFN-g*, *IL-1* gene cluster (*IL-1a*, *IL-1b*, *IL-1R*, *IL-1Ra*), *IL-*

2, *IL-4*, *IL-4Ra*, *IL-6*, *IL-12*, *IL-10*, and *TGF-b*. IL-10 gene variants were confirmed by resequencing through Sanger's method. Multivariate analysis using Competing risk, Kaplan-Meir (with Log-rank test) and Cox-regression survival analyses were performed.

Results: In the allogeneic HCT cohort, HCT recipients receiving a graft from the donors carrying high producer genotype of IL-10 (-1082GG) were strongly protective against grade II-IV acute GVHD (p=0.005) and significant GVHD (p=0.001). In the renal transplant cohort, recipients carrying high IL-10 producing genotypes had significantly better graft survival than recipients carrying low IL-10 producing genotypes (92% v/s 65%; p=0.001).

Conclusions: Genetic predisposition to high IL10 production strongly protects against complications linked to posttransplant allo-immune responses. While HCT recipients receiving grafts from high IL-10 producing donors have a lower incidence of GVHD, renal transplant recipients carrying high IL-10 genotypes have significant better allograft survival. The likely explanation is high IL-10 production contributes to an efficient regulatory immune environment leading to controlled allo-immune responses. These results implicate the importance of assessment of IL-10 gene variants in improving transplant outcomes (e.g., during allogeneic HCT donor selection).

1833 Precision of Mutation Variant Allele Fraction Calculation by Droplet Digital PCR

Drew Williamson[1], Fei Dong[1], Lynette Sholl[1], Jacqueline Bruce[1], Sean Marris[1], Vanesa Rojas-Rudilla[1]
[1]Brigham and Women's Hospital, Boston, MA

Disclosures: Drew Williamson: None; Fei Dong: None; Lynette Sholl: *Consultant*, LOXO Oncology; Jacqueline Bruce: None; Sean Marris: None; Vanesa Rojas-Rudilla: None

Background: Droplet digital PCR (ddPCR) nanofluidic systems can be used to detect somatic mutations to assess cancer burden and guide targeted therapy. However, accuracy of ddPCR depends on multiple factors, including mutation variant allele fraction (VAF) and DNA input concentration, and the analytical framework for calculating uncertainty in VAF quantitation is not well established.

Design: To measure *EGFR* mutation status, we use dual-channel ddPCR to detect *EGFR* wild type and *EGFR* L858R templates and quantitate VAF using a Poisson approximation. Binomial distributions and a Gaussian approximation were used to calculate confidence intervals. Calculated confidence intervals were validated using *in silico* simulations, and accuracy at defined parameters was tested *in vitro*.

Results: We validated our VAF and CI estimations with both *in silico* and *in vitro* experiments. In an *in silico* model of 100 iterations of 15,000 droplets with VAF ranging from 0.1% to 50%, 83% of all predicted VAF values fell within 10% of the true VAF, with loading concentrations ranging from 0.01 to 7.00 mean *EGFR* alleles per droplet. The greatest relative error occurred when both VAF and loading concentration were low, as demonstrated in Figure 1. *In vitro* experiments with VAF ranging from 0 to 10% and loading concentration ranging from 0.14 to 2.47 EGFR alleles per droplet showed increased accuracy at higher loading concentrations, an effect which is most pronounced at samples with low mutation VAF.

Figure 1 - 1833

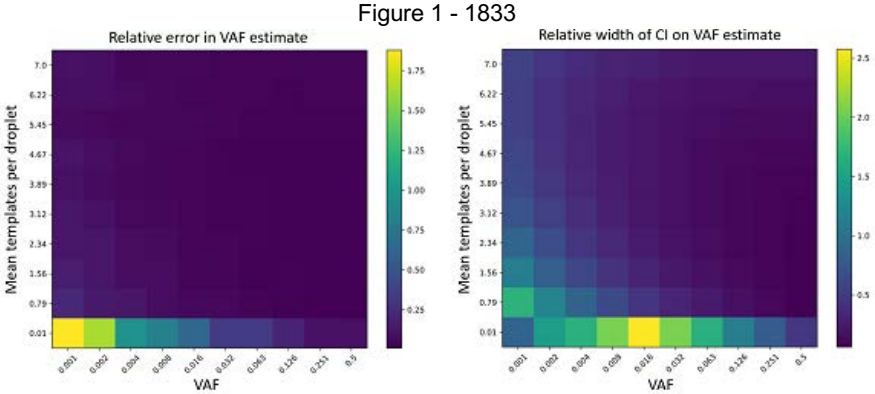

Figure 1: Heatmaps of results of *in silico* model of ddPCR, associating mutation variant allele fraction with DNA input concentration. Left, the mean relative error between true and predicted VAF over 100 iterations. Right, the mean relative width of the calculated CI around our VAF estimate. In both calculations, increasing concentration yields more accurate and less uncertain results.

Conclusions: In specimens with low mutation variant allele fractions, the accuracy of quantitation by ddPCR improves with increasing input concentration away from limiting dilution. This work offers methods for reliable quantification of uncertainty in VAF for ddPCR assays detecting somatic mutations. Accurate calculation of uncertainty in ddPCR provides laboratories with guidelines for optimal loading of input DNA for accurate detection of mutations and offers clinicians additional information that can inform decisions to alter treatment or to resample.

1834 Silencing of MCM7 Promotes Pancreatic Cancer Chemosensitivity through Regulating DNA Damage Response

Jie Yan[1], Jie Chen[2], Min Li[3], Jingxuan Yang, Mingyang Liu[3], Xiaoguang Ren[4], Congwei Jia[2], Shuangni Yu[2], Zhaohui Lu[5]
[1]Peking Union Medical College Hospital, Beijing, China, [2]Peking Union Medical College Hospital, Peking Union Medical College, Chinese Academy of Medical Sciences, Beijing, China, [3]The University of Oklahoma Health Sciences Center, Oklahoma City, OK, [4]Shanghai Medical College, Fudan University, Shanghai, China, [5]Peking Union Medical College, Chinese Academy of Medical Sciences, Beijing, China

Disclosures: Jie Yan: None; Jie Chen: None; Min Li: None; Jingxuan Yang: None; Mingyang Liu: None; Xiaoguang Ren: None; Congwei Jia: None; Shuangni Yu: None; Zhaohui Lu: None

Background: Sustaining proliferation is one of the hallmarks of cancer. We have previously shown that a DNA replication licensing factor MCM7 was a powerful predictor of progression in human pancreatic neuroendocrine tumors. However, the functional role of MCM7 in pancreatic exocrine cancer remains elusive.

Design: We conducted immunohistochemistry staining of MCM7 in a training cohort, which including multi histological types of pancreatic diseases (N=58), and 57 paired pancreatic adenocarcinoma (PDAC) cases with follow-up data. To investigate the biological role of MCM7, the endogenous expression levels of MCM7 were tested in normal pancreatic ductal cell line HPDE and six pancreatic cancer cell lines. EdU staining, cell cycle, cell apoptosis assays and cell viability under gemcitabine treatment were performed in three pancreatic cancer cell lines with MCM7 loss of function. Moreover, 3 X 10^6 MIA shMCM7 or MIA shNC stable cells were injected to the flank of mice respectively (for each group n=10). After one week of implantation, mice were randomly allocated into two sub-groups (n=5). One sub-group received gemcitabine (25 mg/kg, twice-weekly by i.p. injection), and the other group treated with the same amount of PBS.

Results: MCM7 was overexpressed in pancreatic cancer. In PDAC and metastasis lesions, the average label index score of MCM7 was 34.9$\pm$20.7, compared with 2.5 (1.5-4) in benign and precancerous pancreatic tissues. Moreover, the upregulated MCM7 was associated with high pathological grade (P<0.001) and poor prognosis (P<0.001). We also compared the performance of MCM7 with another classical proliferation biomarker Ki-67. The values of area under the ROC curve (AUC) for MCM7 and Ki-67 were 0.96 and 0.95, respectively (both P<0.001).

Silencing MCM7 by two independent siRNAs or shRNAs inhibited PDAC cells proliferation in PANC-1, MIA PaCa-2 and PL45 cell lines. This phenotype was mainly induced by cell cycle dysregulation, rather than cell apoptosis. DNA damage markers, such as phospho-histone H2A.X, phosho-ChK2, were significantly upregulated under gemcitabine treatment in MCM7 silencing cell lines. Consistently, it was obvious that tumor injected with MIA CaPa-2 shMCM7 stable cell lines reduced significantly when treated with gemcitabine comparing with other controls.

Table 1. Association between MCM7 expression and clinical-pathological features of 57 paired PDAC tissues

Characteristics	Number of cases (%)	MCM7 expression (validation cohort)		χ^2	*P*-value
		High	Low		
		Number of cases	Number of cases		
Gender					
Male	35 (61.4)	23	12	1.386	0.239[a]
Female	22 (38.6)	11	11		
Age (years)					
< 65	25 (43.9)	16	9	0.350	0.554[a]
≥ 65	32 (56.1)	18	14		
Location					
Head	38 (66.7)	23	15	0.036	0.849[a]
Body-Tail	19 (33.3)	11	8		
Tumor size (cm)					
< 5	41 (71.9)	22	19	2.178	0.140[a]
≥ 5	16 (28.1)	12	4		
Adjacent organ invasion					
Positive	34 (59.6)	20	14	0.024	0.877[a]
Negative	23 (40.4)	14	9		
Neurovascular invasion					
Positive	33 (57.9)	19	14	0.140	0.708[a]
Negative	24 (42.1)	15	9		
Pathological grade					
I-II	35 (61.4)	15	20	**10.623**	**0.001**[*,a]
III	22 (38.6)	19	3		
T classification					
T1-T2	19 (33.3)	11	8	0.036	0.849[a]
T3	38 (66.7)	23	15		
N classification					
N0	31 (54.4)	17	14	0.653	0.419[a]
N1	26 (45.6)	17	9		
M classification					
M0	53 (93.0)	31	22	0.015	0.904[b]
M1	4 (7.0)	3	1		
AJCC staging (7th edition)					
Stage 1B and Stage 2A	30 (52.6)	16	14	1.050	0.306[a]
Stage IIB and Stage 4	27 (47.4)	18	9		
Vital states (at follow-up)					
Alive	13 (22.8)	2	11	**13.709**	***P*<0.001**[*,a]
Dead	44 (77.2)	32	12		
Follow up (month)	9 (5-25.5)				

*$P<0.05$; Asymptotic significance (two-sided)

[a] χ^2 test

[b] Continuity Correction due to the minimum expected count less than 5

Figure 1 - 1834

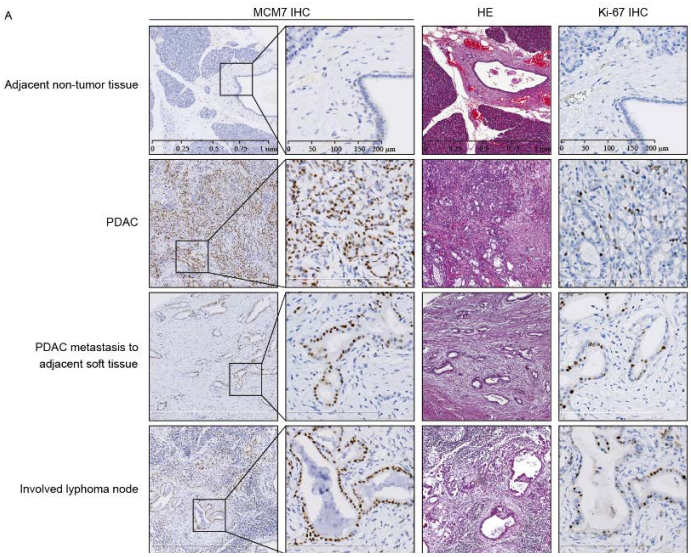

Conclusions: Collectively, this study suggests MCM7 could participate in gemcitabine treatment response and serve as a biomarker for prognosis in pancreatic exocrine cancer.

1835 Prognostic Model for Pancreatic Cancer Based on Dysregulated Transcriptome Analysis

Jie Yan[1], Jie Chen[2], Liangcai Wu[3], Congwei Jia[2], Shuangni Yu[2]
[1]Peking Union Medical College Hospital, Beijing, China, [2]Peking Union Medical College Hospital, Peking Union Medical College, Chinese Academy of Medical Sciences, Beijing, China, [3]Peking Union Medical College, Chinese Academy of Medical Sciences, Beijing, China

Disclosures: Jie Yan: None; Jie Chen: None; Liangcai Wu: None; Congwei Jia: None; Shuangni Yu: None

Background: Pancreatic cancer (PC) is currently one of the most malignant solid tumors, although considerable progress of chemotherapy and targeted therapy have been made over the past decades, it is still hard to identify the patients who may benefit from aggressive adjuvant therapy, therefore, more accuracy prognostic biomarkers for PC are needed.

Design: Seven microarray datasets from Gene Expression Omnibus (GEO), PC sequencing data from Genotype-Tissue Expression (GTEx) and The Cancer Genome Atlas (TCGA) were used to screen differentially expressed genes (DEGs) between PC patients and healthy control samples. Gene ontology (GO) and Kyoto Encyclopedia of Genes and Genomes (KEGG) pathway analyses were applied for the DEGs. The clinical data of PC from TCGA were used to assess the genotype-phenotype association by weighted gene co-expression network analysis (WGCNA). Moreover, PC samples (N=176) from TCGA were randomly divided into a training cohort (N=88) and a validation set (N=88), firstly, the prognosis-related genes were screened to construct prognosis model using Univariate Cox regression analysis and Lasso regression in the training cohort, secondly, the survival-dependent receiver operating characteristic (ROC) curve was used to validate the predictive power of prognosis model in TCGA validation cohort and another microarray cohort (GSE62452).

Results: In this study, a total of 542 DEGs were identified including 369 up-regulated genes and 173 down-regulated genes. GO analysis suggested that the tumor immune microenvironment (TIME) was significantly altered in PC. In WGCNA analysis, comparing with other clinical features, such as age, gender, grade and TNM classification, the survival status was the most significant genes enriched (three out of 14 modules) phenotype. Subsequently, the prognosis significance was analyzed. In Cox's proportional hazards regression model, a prognosis marker model was constructed as: Expression level of *DSG3* * 1.2 + Expression level of *MET* * 2.0. Then, the verification results indicated the Area Under Curves (AUC) for 3-year survival in TCGA validation cohort and GSE62452 were 0.671 and 0.824, respectively.

Table 1 Enrolled PDAC cases from seven GEO datasets after quality control

Country	Organization name	Series	Platform	Normal	Tumor	Quality control
USA	University of Los Angeles	GSE32676	GPL570	7	25	Passed
USA	Mayo Clinic	GSE16515	GPL570	16	36	Passed
USA	University of Florida	GSE71989	GPL570	8	13	Excluded one human chronic pancreatitis tissue
Romania	ICI	GSE15471	GPL570	35	36	Excluded one normal tissue
Italy	Sapienza University of Rome	GSE41368	GPL6244	6	6	Passed
USA	NCI/NIH	GSE28735	GPL6244	44	43	Excluded one normal and two tumor samples
USA	National Cancer Institute	GSE62452	GPL6244	61	67	Excluded two tumor samples

ICI: National Institute for Research in Informatics

Figure 1 - 1835

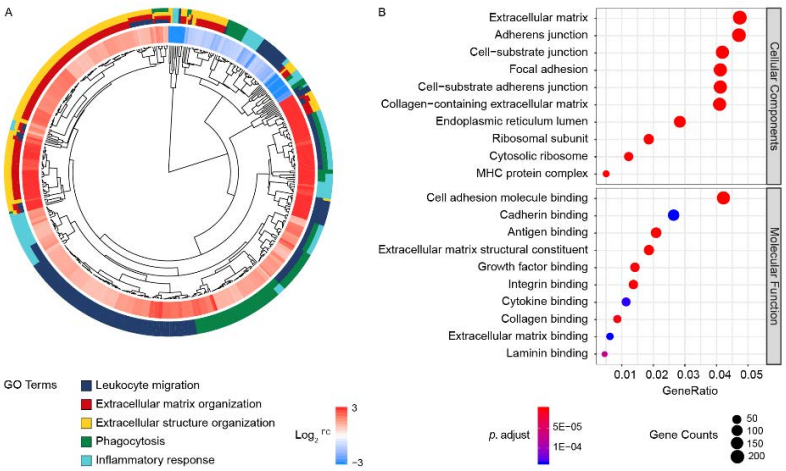

Conclusions: Our results indicated the majority of DEGs may be involved in regulating TIME in PC, and the prognosis model was supposed to improve the prediction of postoperative risk.

1836 Comparative Proteomic Analysis of Breast Implant-Associated Anaplastic Large Cell Lymphoma and Anaplastic Lymphoma Kinase-Positive Anaplastic Large Cell Lymphoma

Guang Yang[1], Özlem Önder[2], Rui Wu[2], Suzanne Turner[3], Kojo Elenitoba-Johnson[4], Megan Lim[5]
[1]The Hospital of the University of Pennsylvania, Philadelphia, PA, [2]University of Pennsylvania, Philadelphia, PA, [3]University of Cambridge, Cambridge, United Kingdom, [4]Perelman School of Medicine at University of Pennsylvania, Philadelphia, PA, [5]Hospital of the University of Pennsylvania, Philadelphia, PA

Disclosures: Guang Yang: None; Özlem Önder: None; Rui Wu: None; Suzanne Turner: None; Kojo Elenitoba-Johnson: None; Megan Lim: None

Background: Breast implant-associated anaplastic large cell lymphoma (BIA-ALCL) is a rare form of anaplastic lymphoma kinase (ALK) negative CD30+ T-cell lymphoma. BIA-ALCL has a genetic and cytokine profile consistent with interleukin 17-producing T-cells (Th17 T-cells) and the JAK-STAT3 pathway is constitutively activated in BIA-ALCL. We compared the proteomic profiles of BIA-ALCL and ALK-positive (ALK+) ALCL using CD4+ T cells as control and sought to characterize the proteome and identify protein biomarkers of BIA-ALCL.

Design: We conducted a mass spectrometry-based, label-free, semi-quantitative comparative whole proteomic analysis by using a BIA-ALCL cell line (TLBR-1), ALK+ ALCL cell line (SUDHL1) and normal human CD4+ T cells. One biologic and technical triplicate experiments were performed. Student's T test were used to test statistically significant differences. KEGG pathway analysis was used to annotate functional categories of differentially expressed proteins.

Results: In total, 1362 out of 1914 proteins (71.2%) were significantly differentially expressed (>2-fold) between TLBR-1 and SUDHL1 cell lines. Among the 503 proteins showing >2-fold increased expression in TLBR-1, THY1 and IL4I1 associated with Th17 T-cells function, as well as STAT6 were significantly increased (1191.0, 296.8 and 66.5-fold, respectively) compared to SUDHL1. These three proteins also showed significantly higher expression (∞, 50.3, 2.6-fold) in TLBR-1 compared to CD4+ T cells. Moreover, we identified proteins that were unique and selectively overexpressed in ALK+ ALCL, including ALK (100-fold), PTPN12 (3.6-fold), SERPINA1 (67.8-fold) and CEBPB (24.5-fold) that are pathogenetically relevant in ALK+ ALCL relative to TLBR-1 and not detected in CD4+ T cells.

Conclusions: Our studies reveal that the proteome profiles of BIA-ALCL are distinct from those of ALK+ ALCL and CD4+ T cells. We identified Th17-related proteins IL4I1 and THY1, and STAT6, which are significantly over-expressed in BIA-ALCL relative to ALK+ ALCL and normal CD4+ T cells suggesting that they may play a role in the pathogenesis and potentially be used as diagnostic biomarkers. Validation of these findings are being performed using western blot, flow cytometry and immunohistochemistry.

1837 Utility of NGS Assessment of Somatic Mutations in Mismatch Repair Genes in Solid Tumors: Improved Overall Survival in Stage III or IV Patients Treated with Immune Checkpoint Blockade

Richard Yang[1], Mustafa Abdulrazzaq[1], Arash Ronaghy[1], Galina Feinstein[1], Victor Prieto[1], L. Jeffrey Medeiros[1], Rajyalakshmi Luthra[1], Keyur Patel[1], Scott Kopetz[1], Russell Broaddus[2]

[1]The University of Texas MD Anderson Cancer Center, Houston, TX, [2]University of North Carolina School of Medicine, Chapel Hill, NC

Disclosures: Richard Yang: None; Mustafa Abdulrazzaq: None; Arash Ronaghy: None; Galina Feinstein: None; Victor Prieto: None; L. Jeffrey Medeiros: None; Rajyalakshmi Luthra: None; Keyur Patel: None; Scott Kopetz: None; Russell Broaddus: None

Background: Microsatellite instability high status (MSI-H) by PCR or deficient mismatch repair (dMMR) expression by IHC are FDA approved indications for treatment with pembrolizumab. Somatic mutations in mismatch repair genes (MMR), namely *MLH1, PMS2, MSH2, MSH6* (SM-MMR), as assessed by next generation sequencing (NGS) is not currently an approved indication for immune checkpoint blockade (ICB) therapy. We interrogated the feasibility of using standardly reported NGS data, particularly the presence of somatic mutations in MMR genes, to determine whether patients with this genetic aberration may be benefitting from ICB therapy.

Design: We filtered our NGS report databases of Oncomine version STGAv1 (n=4,942), STGAv3 (n=4,621), and CMS400 reports (n=556) for cases that harbored a somatic mutation in *MLH1, MSH2, MSH6,* and/or *PMS2*. These solid tumor panels used germline subtraction to filter out SNPs. Limited regions within *MLH1* and none of the regions within *PMS2* and *MSH6* were included in the first version of the STGA panel. We annotated AJCC 8th edition clinical stage, treatment history of ICB therapy (including any anti-PD-1, PD-L1 or CTLA-4 monoclonal antibody), and overall survival of patients starting from the NGS report lock (sign out) date. Kaplan-Meier curves and Mantel-Haenszel statistics were performed in GraphPad Prism v8.1.2.

Results: Overall 267 of 10,119 reports (2.64%) revealed somatic mutations in MMR genes (Table 1). Of these 267 cases, 24 (8.99%) had more than one somatic mutation in MMR genes. Of the 267, 37 patients (16.1%) had stage I or II disease. In advanced solid tumor (stage III or IV) patients, we report here a survival advantage in a set of 178 patients with somatic mutations in MLH1, PMS2, MSH2, and/or MSH6 in their NGS reports. We found a hazard ratio of 2.71 (95% CI 1.65-4.45) in patients treated with ICB compared to patients who received any other therapy (Figure 1). Of these 267 cases, only 40 (15%) were MMR deficient, 69 (25.8%) were MMR intact, and 158 (59.2%) were not tested for MMR by IHC. Of these 267 cases, 13 (4.86%) were MSI-H, 2 (0.75%) were MSI-L, 18 (6.74%) were MSS, and 234 (87.6%) were not tested for MSI by PCR.

	Mismatch Repair (MMR) Gene						
	MLH1	**PMS2**	**MSH2**	**MSH6**	**MMR Mutated Cases**	**Total Cases**	**% SM-MMR**
CMS400	4	1	4	4	**13**	**556**	**2.34**
STGAv1	4	N/A	43	N/A	**47**	**4,942**	**0.95**
STGAv3	42	56	67	66	**207**	**4,621**	**4.48**
Total					**267**	**10,119**	**2.64**

Figure 1 - 1837

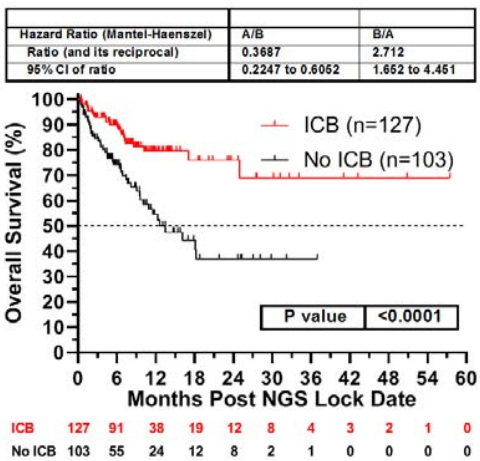

Figure 1. Somatic Mutation in Mismatch Repair (SM-MMR) Genes May Indicate Response to Immune Checkpoint Blockade (ICB). 230 stage III or IV solid tumor patients who harbor a somatic mutation within a mismatch repair genes were annotated for therapy with ICB. Patients who received ICB appeared to have a survival advantage over those treated with other therapy (HR=2.71, 95% CI of 1.65-4.45).

Conclusions: Somatic mutations found in the mismatch repair genes *MLH1, PMS2, MSH2*, and/or *MSH6* by NGS may be a useful predictive biomarker for response to ICB therapy in the future. Also, current practice interrogating MMR by IHC and/or MSI by PCR only found 17.6% of these cases.

1838 Detection of RET Kinase Fusions Using DNA, RNA, and Protein-Based Methods

Soo-Ryum Yang[1], Douglas Mata[2], Ryma Benayed[2], Kerry Mullaney[2], Denise Frosina[2], Natasha Rekhtman[2], Alexander Drilon[2], David Hyman[2], Marc Ladanyi[2], Achim Jungbluth[2], Nino Sireci[3], Jaclyn Hechtman[2]
[1]Department of Pathology, Memorial Sloan Kettering Cancer Center, New York, NY, [2]Memorial Sloan Kettering Cancer Center, New York, NY, [3]Loxo Oncology, Stamford, CT

Disclosures: Soo-Ryum Yang: *Consultant*, Invitae; Douglas Mata: None; Ryma Benayed: None; Kerry Mullaney: None; Denise Frosina: None; Natasha Rekhtman: None; Alexander Drilon: *Advisory Board Member*, Ignyta/Genentech/Roche, Loxo/Bayer/Lilly, Takeda/Ariad/Millenium, TP Therapeutics, AstraZeneca, Pfizer, Blueprint Medicines, Helsinn, Beigene, BergenBio, Hengrui Therapeutics, Exelixis, Tyra Biosciences, Verastem, MORE Health, Abbvie; *Grant or Research Support*, Pfizer, Exelixis, GlaxoSmithKlein, Teva, Taiho, PharmaMar; *Grant or Research Support*, Foundation Medicine; *Consultant*, Wolters Kluwer; *Speaker*, Medscape, OncLive, PeerVoice, Physicians Education Resources, Targeted Oncology, Research to Practice, Oncology; David Hyman: *Stock Ownership*, Fount; *Consultant*, AstraZeneca; *Consultant*, Boehringer Ingelheim; *Consultant*, Pfizer; *Consultant*, Bayer Pharmaceuticals; Marc Ladanyi: None; Achim Jungbluth: None; Nino Sireci: *Employee*, Loxo Oncology, a wholly owned subsidiary of Eli Lilly; Jaclyn Hechtman: *Speaker*, WebMD; *Grant or Research Support*, Eli Lilli

Background: Patients with cancers harboring *RET* kinase fusions demonstrate deep and durable responses to RET-selective targeted therapy. Detection of *RET* fusions is performed using multiple assays and continues to evolve. Here, we compare the performance of several assays in a large pan-cancer cohort.

Design: Tumors were screened for *RET* structural variants (SVs) (e.g., translocations, inversions, deletions, duplications) using a targeted DNA-based sequencing assay (DNA-seq) covering introns 7-11 and all exons in *RET*. *RET* SVs without known 5' partners were classified as SVs of unknown significance (SVUS) and analyzed by a targeted RNA-based sequencing assay (RNA-seq) covering RET exons 8-13. RET immunohistochemistry (IHC) (Abcam EPR2871) was performed in a subset.

Results: *RET* SVs were identified in 0.4% (145/39,217) of all solid tumors analyzed with DNA-seq. Specifically, 120 (83%) had known 5' partners whereas the remaining 25 (17%) were SVUS (Figure 1). On RNA-seq, 56% of the SVUS did not form kinase fusion transcripts, 28% produced kinase fusion transcripts with known 5' partners on RNA-seq only, and 16% were transcribed into kinase fusions with novel 5' partners. After combining all the novel and recurrent kinase fusions, the most common 5' partners were *KIF5B* (46%), *CCDC6* (30%), and *NCOA4* (11%). Primary sites included lung (68%), thyroid (22%), and colorectum (4%), among others. *RET* SVUS that were transcribed into kinase fusions had higher paired-end reads and were more likely contain breakpoints in *RET* intron 11 on DNA-seq (Table 1). To explore the potential utility of IHC for *RET* fusion detection, RET IHC was performed on a subset of canonical *RET* fusion cases (n=19) and a negative control group (n=18). Any cytoplasmic staining was considered positive. 90% of *RET*-fusion positive cancers were positive for RET IHC. The majority (53%) demonstrated diffuse staining with variable intensity (1+ to 3+). 89% of cases without *RET* fusions lacked cytoplasmic staining with a few cases showing apical, membranous staining only (Figure 2). *KIF5B* fusions had higher staining intensity (≥2+) than those with other 5' partners (P = 0.003).

Table 1. Molecular characteristics of DNA-level *RET* SVUS that were non-productive vs. those that were transcribed into kinase fusions on subsequent RNA sequencing.

	RET SVUS without fusion transcripts (n=14)	*RET* SVUS with fusion transcripts (n=11)	P value
Structural variant class			0.03‡
Inversion	8 (57.0%)	1 (9.1%)	
Translocation	3 (21.5%)	7 (63.6%)	
Duplication	0	0	
Deletion	3 (21.5%)	3 (27.3%)	
Median paired-end read count (range)	9.5 (2-131)	38 (19-193)	0.008†
5' partner mapped to intergenic region	9 (64.3%)	4 (36.4%)	0.2‡
RET breakpoint in intron 11	5 (35.7%)	10 (90.9%)	0.01‡
RET kinase domain included	10 (71.4%)	9 (81.8%)	0.7‡
Predicted to form an in-frame fusion	0	3 (27.3%)	0.07‡

SVUS: Structural variants of unknown significance, †Mann–Whitney U Test, ‡Fisher's Exact Test.

Figure 1 - 1838

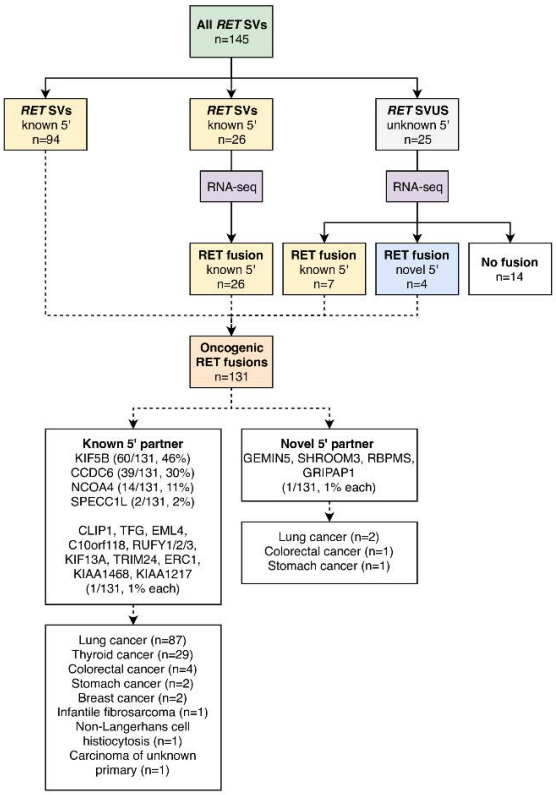

Figure 2 - 1838

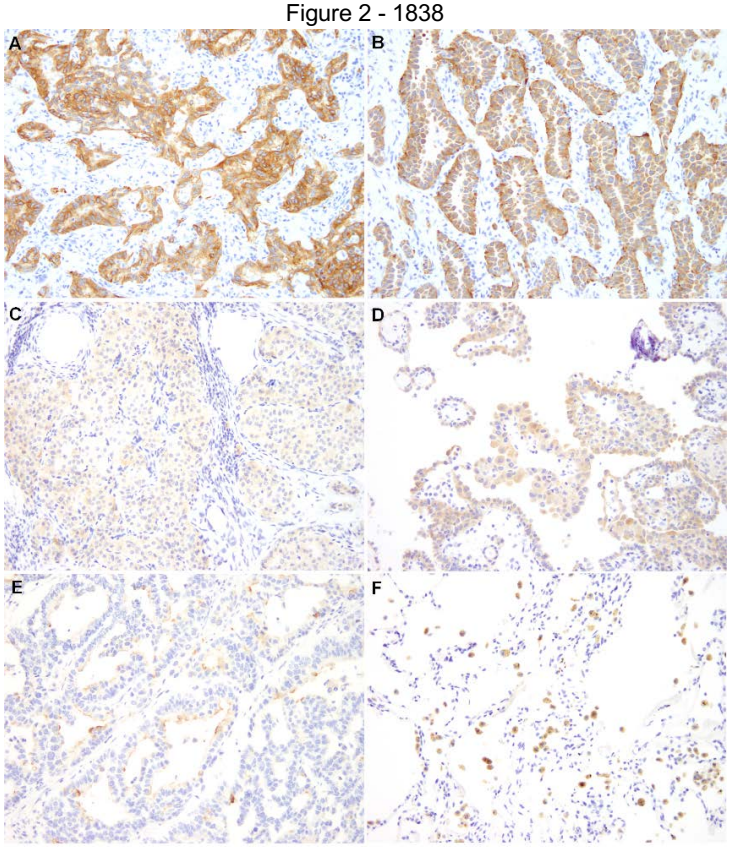

Figure 2: RET immunohistochemistry performed on *RET*-fusion positive (n=19) and negative (n=18) cases. Fusion positive cases included *RET* fusions with *KIF5B* (47%, n=9), *CCDC6* (42%, n=8), and *NCOA4* (11%, n=2). (A,B) *KIF5B-RET* lung adenocarcinomas showing diffuse, 2-3+ cytoplasmic staining. (C) *NCOA4-RET* and (D) *CCDC6-RET* papillary thyroid carcinoma showing patchy 1-2+ cytoplasmic staining. (E) Lung adenocarcinoma negative for *RET* fusion showing patchy, 2-3+ apical and membranous but not cytoplasmic staining. (F) Lung parenchyma with 3+ staining of normal alveolar macrophages and some normal pneumocytes but not in tumor cells.

Conclusions: A subset of *RET* SVs does not result in oncogenic kinase fusions and likely represents non-productive bystander events. Hence, caution is required when using DNA-based assays. Nearly half of SVUS produce kinase fusion transcripts, highlighting the need for confirmatory testing. The diagnostic utility of RET IHC is promising, and further validation is ongoing.

1839 Histomorphologic, Immunohistochemical and Molecular Validation of 2.5-Hour Processed Large Specimens/Tumor Resections with Tissue-Tek Xpress x120

Richard Zarbo[1], Margeaux Schmidt[1], Nathan Althaver[1], Lisa Whiteley[2], Nilesh Gupta[2], Dhananjay Chitale[3], Dayna Goerke[1]
[1]Henry Ford Hospital, Detroit, MI, [2]Henry Ford Health System, Detroit, MI, [3]Henry Ford Hospital, West Bloomfield, MI

Disclosures: Richard Zarbo: None; Margeaux Schmidt: None; Nathan Althaver: None; Lisa Whiteley: None; Nilesh Gupta: None; Dhananjay Chitale: None; Dayna Goerke: None

Background: We seek to shorten histology preanalytic time to meet pathology reporting needs of 16 weekly specialty Tumor Boards in the precision medicine oncology program of the Henry Ford Cancer Institute.

Design: We validated an extended 2.5-hour microwave and vacuum-assisted processing cycle (Tissue-Tek Xpress *x120*, Sakura Finetek USA, Torrance, CA) for large specimens/tumor resections compared to our 5.5-10 hour microwave process (Logos, Milestone, Kalamazoo, MI). Specimens were collected from operating rooms of Henry Ford Hospital, dissected fresh at 2-3mm thickness into mirror images and fixed in 10% neutral buffered formalin, minimum 6, maximum 72 hours. Xpress bench processing step post formalin fixation was 30 minutes of isopropranol-based pre-processing solution for water/formalin extraction followed by 2 hours of Xpress processor time composed of 2 x 30-minute microwave temperature controlled isopropyl alcohol and acetone based dehydration/xylene-free clearing retorts and 2 x 30-minute heated paraffin impregnation retorts using vacuum. Blocks from both Xpress and Logos pathways were cut and stained together to minimize inter-run variation. 3 pathologists assessed slides for histomorphology (188 tumor and 67 normal tissues), and 24

selected tumors in a tissue microarray (TMA) (2 cores from each tumor: 10 lung, 10 colon, 4 renal cell) for immunohistochemical (IHC) staining with 22 antibodies and molecular validation of DNA/RNA quality and next generation sequencing (NGS) assay using TruSeq Amplicon 48-gene Cancer Panel (Illumina, San Diego, CA).

Results: All tissues were equivalent for histologic interpretation. There were no differences in IHC profiles of TMA tissues for PAX5, PAX8, CD45, CD3, CD10, CD20, TTF-1, Napsin A, CK5/6, CK7, cytokeratins AE1/AE3, CAM 5.2, p63, p40, EMA, vimentin, carbonic anhydrase IX, AMACR, CDX2, Ki67, and beta catenin. DNA/RNA quality between the 2 processors was comparable (Table 1a, 1b) as was quality of DNA/RNA purity and amplicon fragment length (200, 300, 400 bp). There was good correlation between % uniformity of coverage, but poor for depth of coverage. All samples passed NGS quality matrix criteria for reporting variants and no differences in hot spot mutations were detected (Table 2).

Figure 1 - 1839

Table 1a

DNA Quality / quantity	Tissue Tek Xpress X120		Logos	
	DNA Purity	DNA Nanodrop [ng/ul]	DNA Purity-clinical	DNA Nanodrop [ng/ul]-clinical
Average	1.98	62.21	2.09	47.31
Minimum	1.78	4.70	1.74	1.10
Maximum	2.35	158.70	4.73	119.70

Table 1b

RNA Quality / quantity	Tissue Tek Xpress X120		Logos	
	RNA Purity	RNA Nanodrop [ng/ul]	RNA Purity-clinical	RNA Nanodrop [ng/ul]-clinical
Average	2.04	133.44	2.02	130.19
Minimum	1.84	8.30	1.78	3.70
Maximum	2.60	338.70	2.35	453.20

Table 2

NGS Quality matrix	Tissue Tek Xpress X120		Logos	
	Depth of coverage	% uniformity of coverage	Depth of coverage	% uniformity of coverage
Average	9882	91%	9051	87%
Minimum	2259	85%	721	77%
Maximum	15106	98%	14786	91%

Conclusions: This validated Xpress processor for large specimens/tumor resections will reduce current technical process time by 55-75% and promotes our goal of continuous laboratory production flow to meet the demand for faster surgical pathology diagnostic reporting.

1840 Evaluation of T Cell Receptor (TCR) Repertoire by Next-Generation Sequencing (NGS) Based TCR Gamma Chain Clonality Testing

Menglei Zhu[1], Mustafa Syed[1], Wayne Yu[1], Caleb Ho[1], Kseniya Petrova-Drus[1], Khedoudja Nafa[1], Andres Quesada[1], Ahmet Dogan[1], Maria Arcila[1]
[1]*Memorial Sloan Kettering Cancer Center, New York, NY*

Disclosures: Menglei Zhu: None; Mustafa Syed: None; Wayne Yu: None; Caleb Ho: *Speaker*, Invivoscribe, Inc.; Kseniya Petrova-Drus: None; Khedoudja Nafa: *Speaker*, Biocartis; Andres Quesada: None; Ahmet Dogan: *Consultant*, Roche, Corvus Pharmaceuticals, Seattle Genetics, Oncology Specialty Group, Pharmacyclics, Celgene, Novartis, Takeda; *Primary Investigator*, Roche/Genentech; Maria Arcila: *Speaker*, Invivoscribe; *Speaker*, Biocartis

Background: TCRs are highly diverse heterodimers which recognize the antigen-major histocompatibility complex (MHC) to mediate antigen recognition and immune responses. The TCR repertoire is the sum-total of all TCRs expressed in the T cells of an individual which changes dynamically through physiologic, pathologic and treatment states. Integrating studies that allow the interrogation of this highly dynamic system are becoming increasingly important. However, methodology for this assessment is highly variable and not yet standardized for research or routine clinical use. Here, we describe our approach to assessing TCR gamma repertoire.

Design: To establish the methodology to evaluate TCR repertories, we used our clinically validated NGS-based TCR gamma clonality assay which utilizes commercially available primers (Lymphotrack, Invivoscribe) targeting TCR gamma. Clinical samples submitted for clonal characterization and well-characterized control samples were evaluated. DNA was extracted from blood, bone marrow and fresh or formalin-fixed paraffin-embedded tissue (FFPE). Sequencing was performed using Illumina MiSeq instruments following manufacturer's protocols. TCR Repertoire diversity was quantified as follows: Entropy weighed both the number of clonotypes and their relative frequencies in each sample as described previously. Clonality, a related parameter of entropy, was obtained from the normalized entropy of each sample: clonality = 0 when all clones are equal in size and =1 when restriction to a single clone is detected.

Results: Assessment of TCR repertoire was performed on 540 patient samples and 120 control samples. Inter-assay reproducibility is evaluated by testing same control samples in 48 different runs. Inter-assay coefficients of variability (CV) for entropy and clonality are 2% and 12%, respectively. The intra-assay reproducibility was evaluated using duplicate runs of 153 patient samples (Figure 1). The intra-assay CV for entropy and clonality were 0.7% and 7.7%, respectively. Clonality was inversely correlated with the presentation and the size of dominant clone in the samples. Formalin fixation did not significantly interfere with assessment of entropy or clonality.

Figure 1 - 1840

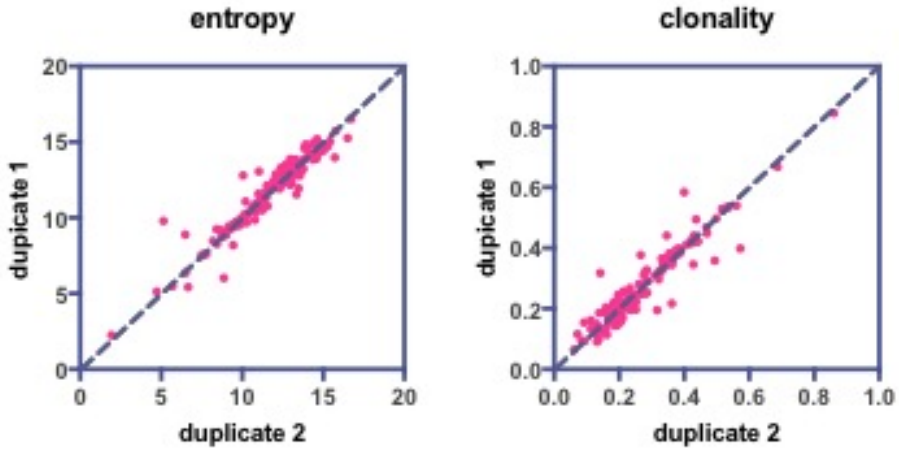

Conclusions: This study shows that clinically validated assays for NGS based clonality testing may be used for assessment of repertoire diversity with high reproducibility and may potentially provide valuable monitoring information. Further efforts for clinical validation and standardization are required.

1841 HCC-derived Extracellular Vesicle Purification for Early-Stage HCC Detection

Yazhen Zhu[1], Na Sun[2], Hsian-Rong Tseng[2]
[1]University of California Los Angeles, Los Angeles, CA, [2]David Geffen School of Medicine at UCLA, Los Angeles, CA

Disclosures: Yazhen Zhu: None; Na Sun: None; Hsian-Rong Tseng: None

Background: The poor prognosis of HCC is due to the fact that diagnosis is often made at a late stage in disease development. It is crucial to develop a non-invasive liquid biopsy-based diagnostic solution for early detection of HCC. This study aimed to develop a new platform (i.e., EV Click Chips) for the purification of HCC-derived extracellular vesicles (EVs) for non-invasive detection of early-stage HCC from at-risk chronic liver diseases (CLD).

Design: Plasma samples of 129 participants from four cohorts were investigated in this study, including (i) healthy donors (HD, n = 24); (ii) patients with at-risk chronic liver disease (CLD) (n = 27); (iii) treatment-naive patients with HCC (n = 40); and (iv) patients with primary malignancies other than HCC, with or without liver metastases (n = 38). The HCC-derived EVs were purified from plasma samples obtained from the 129 participants using the optimized EV Click Chips. Reverse-transcriptase droplet digital PCR (RT-ddPCR) was applied to quantify the expression of 10 well-validated HCC-specific genes in the purified HCC-derived EVs. Logistic regression models were constructed and leave-one-out cross-validation (LOOCV) was performed based on the copy numbers of the 10 genes. The area under the receiver operating characteristic curve (AUC) was used to evaluate the diagnostic accuracy (workflow showed in Fig. 1a).

Results: As depicted in the heat maps, HCC patients are grouped according to Milan Criteria and Barcelona Clinic Liver Cancer (BCLC) staging system (Fig. 1b, upper). Higher signals are observed in HCC patients, compared with the control groups (healthy donors and patients with at-risk chronic liver diseases) (Fig. 1b, Middle), or patients with cancers other than HCC (Fig. 1b, Lower). The HCC EV scores showed differences among different groups, as depicted in the boxplot (Fig. 2a). The AUC for the HCC EV score for differentiating 1) HCC versus Non-HCC is 0.94 and 0.90 before and after LOOCV, respectively (Fig. 2b); 2) HCC versus HD&CLD is 0.94 and 0.88 without and with LOOCV, respectively (Fig. 2c); 3) differentiating HCC versus other cancers is 1.00 and 0.90 without and with LOOCV, respectively (Fig 2d); 4) both early-stage HCC (BCLC stage 0-A) and localized HCC (within Milan criteria) versus at-risk CLD outperformed the AUC for clinical AFP test (0.94 versus 0.77, BCLC, Fig.2e; and 0.97 versus 0.76, Milan criteria, Fig.2f, respectively).

Figure 1 - 1841

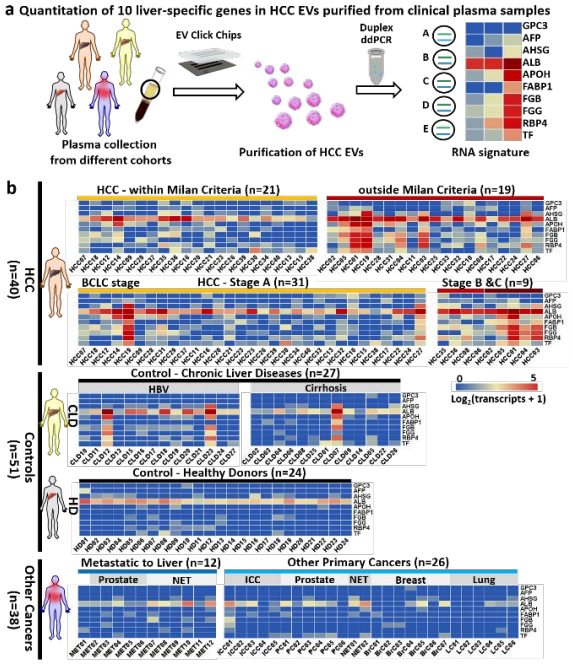

Figure 2 - 1841

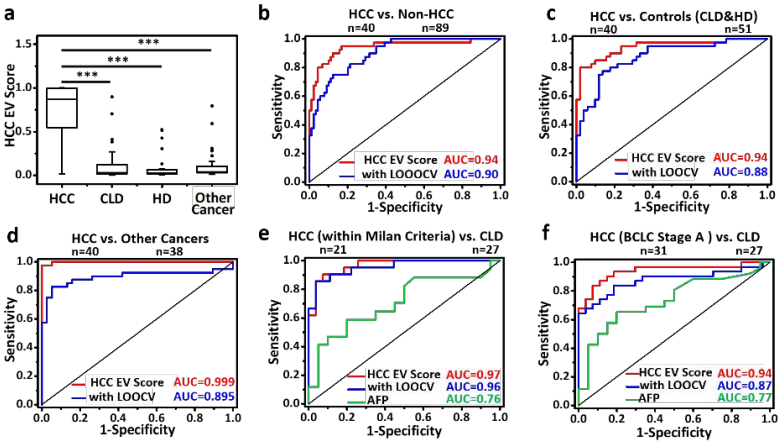

Conclusions: We developed an HCC EV purification platform for the detection of early-stage HCC from at-risk CLD.